18

Obtaining and Indexing Parallel-Beam Diffraction Patterns

CHAPTER PREVIEW

The core strength of TEM is that you can obtain both a DP and an image from the same part of your specimen (not to mention various spectra). To obtain the crystallographic data, a method for interpreting and indexing the DP is essential and this aspect is the theme for the next four chapters. We'll start in this chapter by considering classic selected-area diffraction (SAD) patterns (SADPs) and how to index them, but also introduce other related, if less widely used, parallel-beam diffraction methods.

You can proceed to index your pattern in several ways, depending on how much information you already know about your specimen. We will begin the chapter by considering the experimental approach with the aim of being able to identify shortcuts whenever possible. The experienced microscopist will readily identify many patterns just by looking at them, but will still need to index new patterns or to identify unfamiliar ones. The fastest and most efficient experimental approach may take advantage of several concepts covered in the preceding two chapters and the following three. Today, sophisticated computer software is available which takes much of the tedium out of the indexing process.

Most DPs in a TEM are single-crystal (spot) patterns because the area from which we can routinely obtain SADPs (< 1 μm) is smaller than typical grain sizes of most engineering materials. However, with increased emphasis on nanocrystalline materials (grain size < 0.1 μm), it is more usual for the DPs to contain contributions from many crystals and so ring/textured SADPs are increasingly common. (We'll cover convergent-beam (CBED) and other forms of micro/nanodiffraction patterns, which can come from regions < 10 nm, in Chapters 20 and 21.) Using the DP, we can identify the crystal (which we often already know) and its orientation (which we probably don't) with respect to both the beam and to any adjacent crystals. The positions of the allowed *hkl* reflections are characteristic of the crystal system. Indexing associates each spot or ring in the DP with a plane (*hkl*), or set of planes {*hkl*}, in the crystal. From the indexing of the spots, you can deduce the orientation of the crystal in terms of the zone axis [*UVW*] in which the indexed planes lie.

BEAM DIRECTION

It is convention to define [*UVW*] as the beam direction. This direction is *normal* to the plane of the DP and *anti-parallel* to the electron beam.

If you want to know the orientation relationship between two crystals, you need to know more than one [*UVW*] for each crystal and, as we'll show, it is the determination of orientation relationships between different phases or differently oriented crystals that is the most useful information to come out of DP indexing. Orientation determination in the TEM is so important that we devote a complete chapter to the topic in the companion text. Now, computer control of both DP formation and DP indexing is very much the norm, but if you don't understand the principles, you shouldn't believe the computer output (GIGO). So we deliberately confine our discussion of computer-assisted indexing to the end of this chapter.

18.1 CHOOSING YOUR TECHNIQUE

The technique you choose to study your specimen will depend on what you *want* to learn and what you *can* learn. For example, if you want to learn about the crystal structure of a particular region, diffraction is generally the way to go although you may find moiré fringes (Chapter 23) or HRTEM (Chapter 28) more appropriate. Basically there are three diffraction approaches:

- You can spread the beam to give nearly parallel illumination and then use an aperture to select an area in the first image formed by the objective lens (giving the SADPs of Chapters 9 and 11). We emphasize SAD indexing in this chapter.
- SADPs often contain Kikuchi lines which give more accurate orientation determination (see Chapter 19).
- You can focus the beam on a small area of your specimen to form a CBED pattern (we won't use CBDP) (see Chapters 20 and 21).

SAD ACRONYMS

SADP versus SAD pattern, SAED versus SAD and CBEDP versus CBDP versus CBED pattern. We try to use DP throughout the book but some conventions are very well established!

We can also summarize the possibilities as a function of the grain size of the material. Let's consider this particular specimen characteristic

- The grain size may be very small, $<<10$ nm, typical of many nanocrystalline thin films. This is a problem because it's rare that a single grain will extend through the thickness of your specimen, in which case you can't easily index an individual crystal pattern. (This is the rhino problem (Figure 1.7) for DPs!) However, in this case you probably won't want to know the *orientation* of a particular grain but will instead be interested in knowing the *texture* of the material.
- The grain size is between 10 and ~100 nm. Here CBED may be useful because it gives you a small probe. However, much of the benefit of CBED comes from having specimens which are >100 nm thick; the best thickness depends on the structure factor (atomic number) of your specimen. If you're careful and are using a recent-model TEM in which C_s and λ are small, you might be able to use SAD in this range of grain size, as we saw in Table 11.1.
- The grain size is in the range 100 nm to ~2 μm. In this situation, SAD can be used quite routinely in a modern TEM. You must be aware of the limitations and be prepared to unravel a complex DP. Because of errors due to C_s and Δf, the problem will be distinguishing which spots arise from the area you selected and which spots arise from neighboring areas.
- The specimen is uniformly thin with grain size > 2 μm. This type of specimen is just a simpler version of the last case. You should have no problem in applying SAD techniques even at lower voltages and in older microscopes. Now CBED will be very useful in examining local changes *within* a grain.
- The grains of interest are large (> 2 μm, even better if they are > 5 μm) with both thin areas (< 100–300 nm thick, depending on the material) and areas which are sufficiently thick for Kikuchi lines to be visible (see next chapter). Now you can use any of these techniques, except texture analysis, which becomes more difficult! For the latter, you should now consider the electron-backscatter diffraction (EBSD) technique using a bulk specimen in an SEM to give better statistics (Schwartz et al.).

In this chapter, we'll concentrate on the hands-on approach to SAD analysis and leave CBED to Chapters 20 and 21. We'll also introduce hollow-cone and precession diffraction which make your SADPs more useful at times. We can't give you a foolproof guide since the best technique(s) will depend on your specimen.

18.2 EXPERIMENTAL SAD TECHNIQUES

By now you should know how the experimental camera length (L) compares to the value you read from the microscope. You also know how the SADP is rotated with respect to the image as the magnification changes (unless your particular TEM automatically compensates for this rotation). You've checked that you haven't missed a 180° inversion; leading researchers have missed this in the past. Go back to Sections 9.3–9.6 and 11.9 if you need to refresh the details of the practical steps involved in obtaining SADPs.

You can vary L but your pattern may rotate as you do so. We generally use a value of ~500 mm for SAD, but that will depend on your TEM, whether you want to see detail in the HOLZ and on the interplanar spacings in your specimen. It's good practice to choose a particular value of L and always use that value for your SADPs with a particular instrument/specimen combination. You may want to increase L for special high-resolution diffraction, but you'll give up a large number of other reflections and enlarging the photographic film will almost always provide the magnification you need. This is where a wide-angle CCD camera (Chapter 7) that captures a much larger area of reciprocal space than standard TEM film can be really useful.

Tilting and rotating your specimen. One of the biggest assets of the TEM is that you can monitor the DP as you tilt or rotate your specimen. Rotating the pattern requires a rotation holder (Chapter 8), which is ideal if you want to align a particular reflection parallel to the tilt axis, especially for a side-entry holder. This alignment is particularly helpful in stereomicroscopy (see Chapter 29). Tilting the specimen is far more common than rotating, since all side-entry holders automatically have one tilt axis parallel to the specimen rod. We discussed the importance of eucentricity in Chapter 9.

TILTING

Tilting the specimen changes the diffraction conditions and may change the focus.

It is good practice to note the tilt settings whenever you are recording images. If you want to use these settings to give a rough estimate of how far you're tilting the specimen, you should remember that there may be some backlash due to mechanical hysteresis. So you will always need to approach a particular setting from the same tilt direction if you need to be exact. In the next chapter, we'll describe how we use Kikuchi maps to guide us as we tilt the specimen. If you don't have Kikuchi lines because your specimen is too thin, or too bent, you can still use the idea. Select a particular strongly diffracted beam and then tilt the specimen so that that particular beam remains excited. What you are doing is tilting the specimen so that the same plane remains nearly parallel to the electron beam (think about what this means and the crystallographic information that it can give you).

Tilting the beam. If you are really interested in examining the detail present in the DP and the image is less important, you can change the diffraction conditions in a very controlled and reversible way by tilting the beam using the DF deflection coils. You can be much more precise than mechanical tilting with the goniometer since there is no problem with backlash. To increase your accuracy, you may want to increase L. This technique is particularly helpful when you want to examine the effect of small changes in $\mathbf{s}$ on the appearance of diffraction spots.

For example, if you want to excite the third-order reflection 3**g** in BF, you could use the approach shown in Figure 18.1. (You wouldn't, but this exercise is useful!)

- Use the beam tilt (dark-field deflection coils) to put $\bar{\mathbf{g}}$ on the optic axis (where **0** was) (Figure 18.1A). Now tilt the sample so that **g** is excited. Then tilt the beam to put **0** back on the optic axis. 3**g** is now excited.

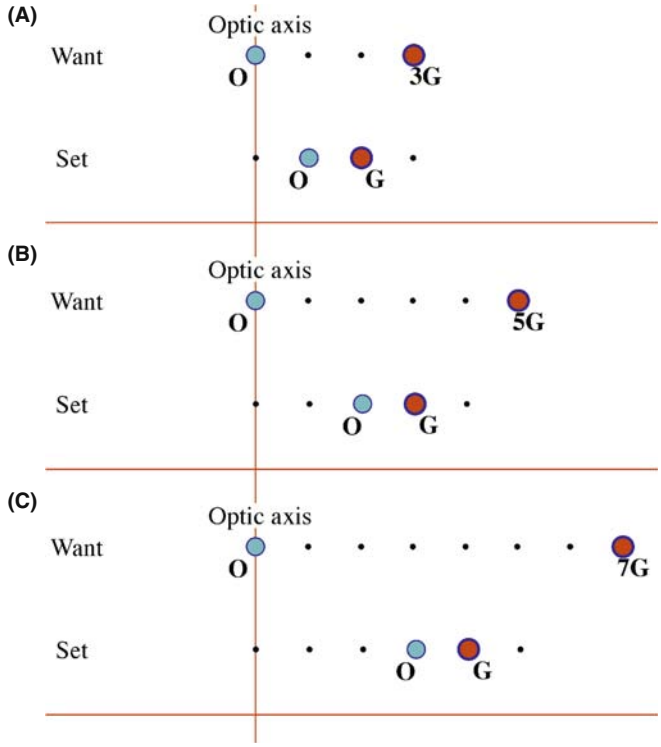

FIGURE 18.1. Exercises in exciting high-order reflections. (A) To excite 3G in BF, tilt the beam so –G is on axis with G strongly excited, then tilt O back onto the optic axis. (B) To excite 5G in BF, tilt the beam so –2G is on axis with G strongly excited, then tilt O back onto the optic axis. (C) To excite 7G in BF, tilt the beam so −3G is on axis with G strongly excited, then tilt O back onto the optic axis.

Next, repeat the exercise but with the aim of exciting 5**g**.

- Use the beam tilt (dark-field deflection coils) to put $2\bar{\mathbf{g}}$ on the optic axis (where **0** was) (Figure 18.1B). Now tilt the sample so that **g** is excited (as before). Then tilt the beam to put **0** back on the optic axis. 5**g** is now excited.

Repeat the exercise again but with the aim of exciting 7**g**.

- Use the beam tilt (dark-field deflection coils) to put $3\bar{\mathbf{g}}$ on the optic axis (where **0** was) (Figure 18.1C). Now tilt the sample so that **g** is excited (as before). Then tilt the beam to put **0** back on the optic axis. 7**g** is now excited.

Now you can see that if you want to excite 11**g**, but you won't be able to see 11**g** on the DP, start by moving $5\bar{\mathbf{g}}$ to the optic axis. You should now appreciate the possibilities.

We'll develop other variations of this technique in Chapter 19, and we'll see in Chapter 27 that the situation in Figure 18.1 does arise in weak-beam microscopy at higher voltages. Computerized control of the beam tilt is essential to hollow-cone and precession diffraction methods which we'll discuss toward the end of the chapter.

18.3 THE STEREOGRAPHIC PROJECTION

DPs not only tell us the direction of the electron beam but also the complete orientation of that region of the specimen illuminated by the beam. If we have a grain boundary or interphase interface (or indeed any planar defect) present in the specimen, we can determine the orientation of both grains and the plane of the interface. As we show in great detail in the companion text, what we often want to know is how the two crystals are related to one another. But first, we need a method for visualizing this relationship; this is where the stereographic projection or stereogram is an invaluable aid. Unfortunately the classic materials texts by Johari and Thomas and by Smaill are out of print, so to get an in-depth appreciation of this technique, you'll have to resort to crystallography texts, such as those listed in the general reference section or a dedicated stereographic-projection text in another field (e.g., Lisle and Leyshon). Like other tools, you'll have to understand it and use it before you fully appreciate its value. We strongly recommend that you take time out to do this if you're not already familiar with the construction. Any introductory crystallography text is a good place to start and several are listed in the references.

The construction. Imagine a crystal located inside a sphere as shown in Figure 18.2. Draw a line normal to each crystal plane from the center of the sphere (the sphere of projection) to intersect the sphere at point P in the northern hemisphere; the cross section view may be easier to visualize. Now draw a second line from the south pole to point P.

This second line cuts the equatorial plane at the point P′. The disk of the equatorial plane is the stereographic projection and the point P′ *uniquely* represents the plane whose radial normal cuts through P. If P is in the southern hemisphere, we draw the line from the north pole instead and identify this P′ on the projection with a circle instead of a dot.

Look again at the crystal; it's cubic to keep it simple but the construction is completely general. The normals to the planes (100), (111), (011) and $(\bar{1}11)$ all lie on the circumference of a circle around the sphere of projection. In this special case, all of the points on this circumference project onto the same great circle on the stereographic projection whose circumference we call the 'primitive' great circle. The Wulff net in Figure 18.3 shows 90 such great circles all passing from the north pole to the south pole and another around the equator: a great circle always passes through opposite ends of a diameter in the projection. These are the familiar lines of longitude on the globe. Circles on the sphere which do not contain the center of the sphere are smaller; they also project as circles called the small

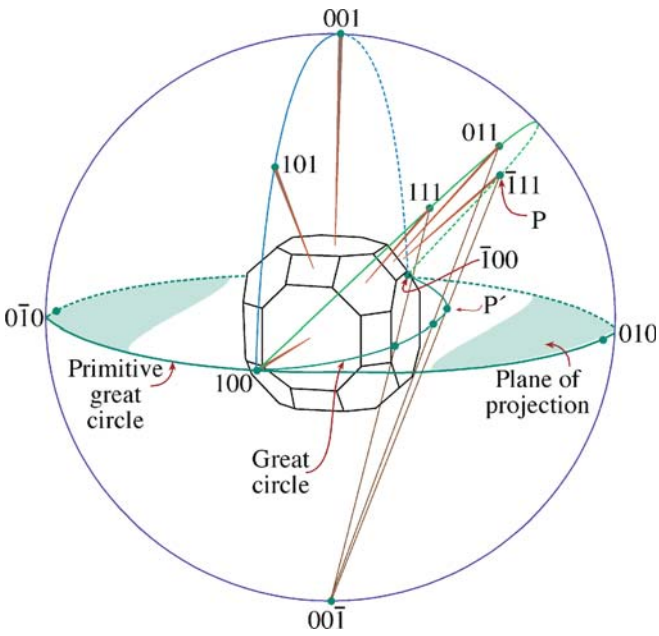

FIGURE 18.2. The stereographic projection. The crystal is at the center of the sphere. Normals to the crystal planes are projected until they intercept the sphere at P, then projected back to the south pole $(00\bar{1})$ of the sphere. Where this projected line crosses the equatorial plane at P' is the point that uniquely represents the original plane in the crystal. Note that planes in the same zone on the crystal project as a great circle in the stereographic projection. An example of such a great circle is its diameter (or line of longitude); another is the circumference in the equatorial plane.

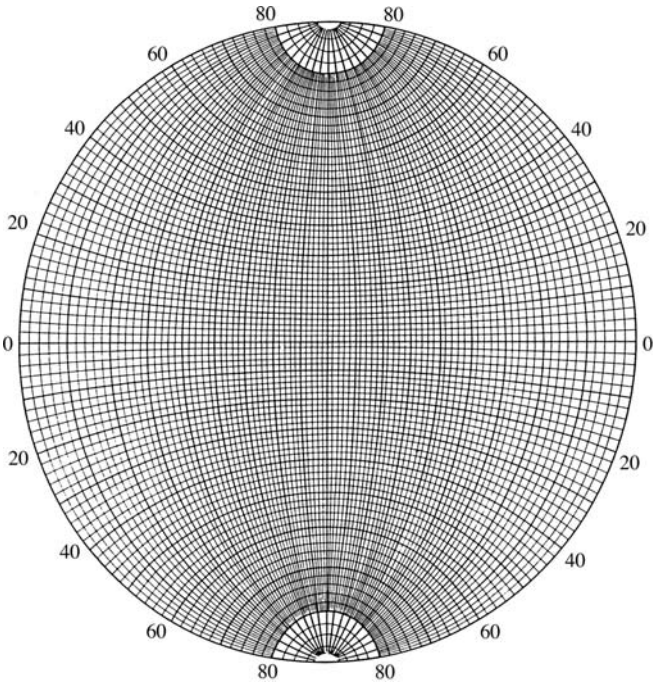

FIGURE 18.3. A Wulff net which contains 90 great circles like the one in Figure 18.2; each great circle is 2° apart so the net covers 180°. The only great circle that actually appears as a circle in the net is the circumference of the projection, called the primitive great circle. Points on the primitive represent planes whose normals are 90° from the north pole (which projects in the center of the Wulff net). Thus all distances on the net are proportional to angles in real space but only correspond exactly to angles around the primitive.

circles which, if concentric with the primitive, are familiar as lines of latitude. (Note, however, that most small circles are not concentric with the primitive.) We can then rotate the Wulff net, as we wish, to realign our great circles.

- We can represent plane normals (also called poles) and directions on the same projection even if they are not parallel to one another. Better still, we can read off the angles between them. Remember that, in general, the normal to the plane (*hkl*) is parallel to the direction [*hkl*] only for cubic materials.
- The zone axis is always 90° away from any plane normal that is in its zone. All the plane normals in a particular zone, [*UVW*], will lie on a single great circle.
- The angle between any two planes is the angle between their plane normals, measured along a great circle using the Wulff net.
- We can use the same construction to summarize all the symmetry elements of any particular crystal system.

These poles at the *UVW* zone axis represent the *possible diffracting planes* for that zone; [*UVW*] is the beam direction. So if [*UVW*] is in the center of the projection, the *hkl* reflections will be around the circumference of the projection (the primitive great circle). Now you should appreciate why stereograms can be so useful in interpreting DPs.

Several examples of stereographic projections are shown in Figure 18.4. Look at the Wulff net and check some simple facts. For example, for the cubic system, check which poles are 90° away from the [001] direction. How large is the angle between $(0\bar{1}1)$ and (011)? How would this angle change if the material were forced to be tetragonal with $c/a > 1$? What happens in this case to the $(1\bar{1}1)$ pole or the $(1\bar{1}0)$ pole? Now consider the more extensive plot shown in Figure 18.5. If the specimen is cubic with the [001] foil normal, what pole would you tilt to if you wanted to form an image with the $0\bar{2}2$ reflection? (One answer is the [011] zone axis, but why?). For the same specimen, if you want to excite the $\bar{1}11$ reflection, you could tilt toward the $[0\bar{1}1]$ zone axis keeping the 200 reflection excited, not toward the [011] zone axis.

- You could work this out using equations, but the stereographic projection tells you what to do while you are sitting at the microscope.
- If you are working with a non-cubic material, buy a large Wulff net and construct your own stereographic projection; you can buy standard projections for cubic materials so, as usual, it's easier to be a metallurgist than a ceramist or mineralogist.
- Use a program like EMS to help you plot the points, or download appropriate software from the Web (e.g., URL #1).
- Wulff nets and plotting software are also available on-line (e.g., URL #2).

18.4 INDEXING SINGLE-CRYSTAL DPs

Remember the fundamental relationship in a DP (Section 9.6.B).

$$Rd = \lambda L \tag{18.1}$$

Any distance between the direct beam and a specific diffraction spot or the radius of a diffraction ring, *R*, which we measure on the DP, is related to a specific spacing between planes in the crystal, *d*. Since λL is a constant, we can measure several values of *R* and know that

$$R_1 d_1 = R_2 d_2 = R_3 d_3 = R_4 d_4 = \ldots \tag{18.2}$$

If you know the lattice parameter of your crystal, then you know the allowed reflections and only certain *d*-spacings will be associated with diffraction spots.

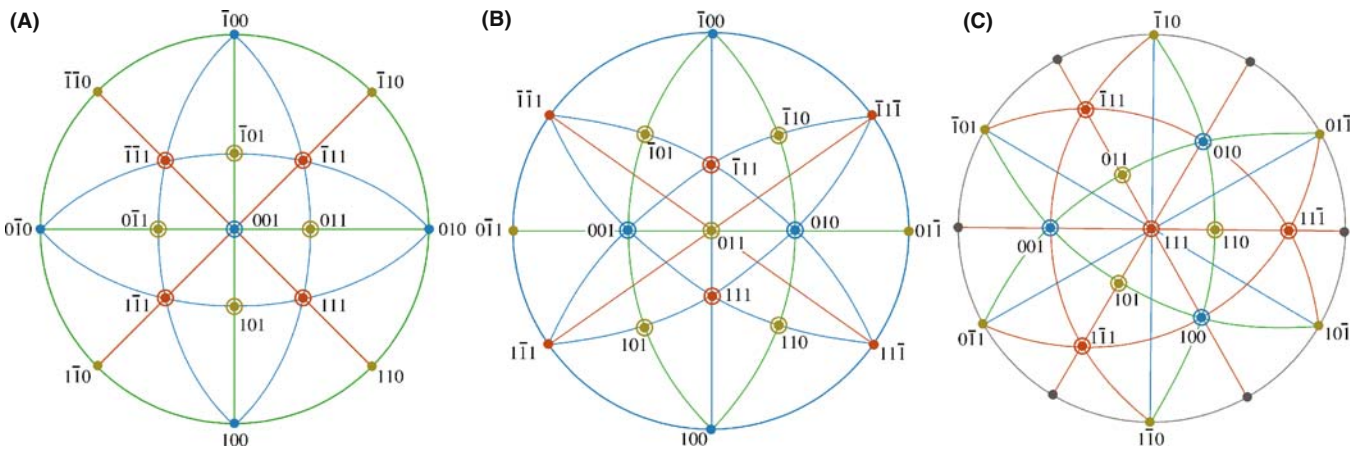

FIGURE 18.4. Some standard cubic stereographic projections. The pole in the center defines each projection, so these are 001, 011 and 111.

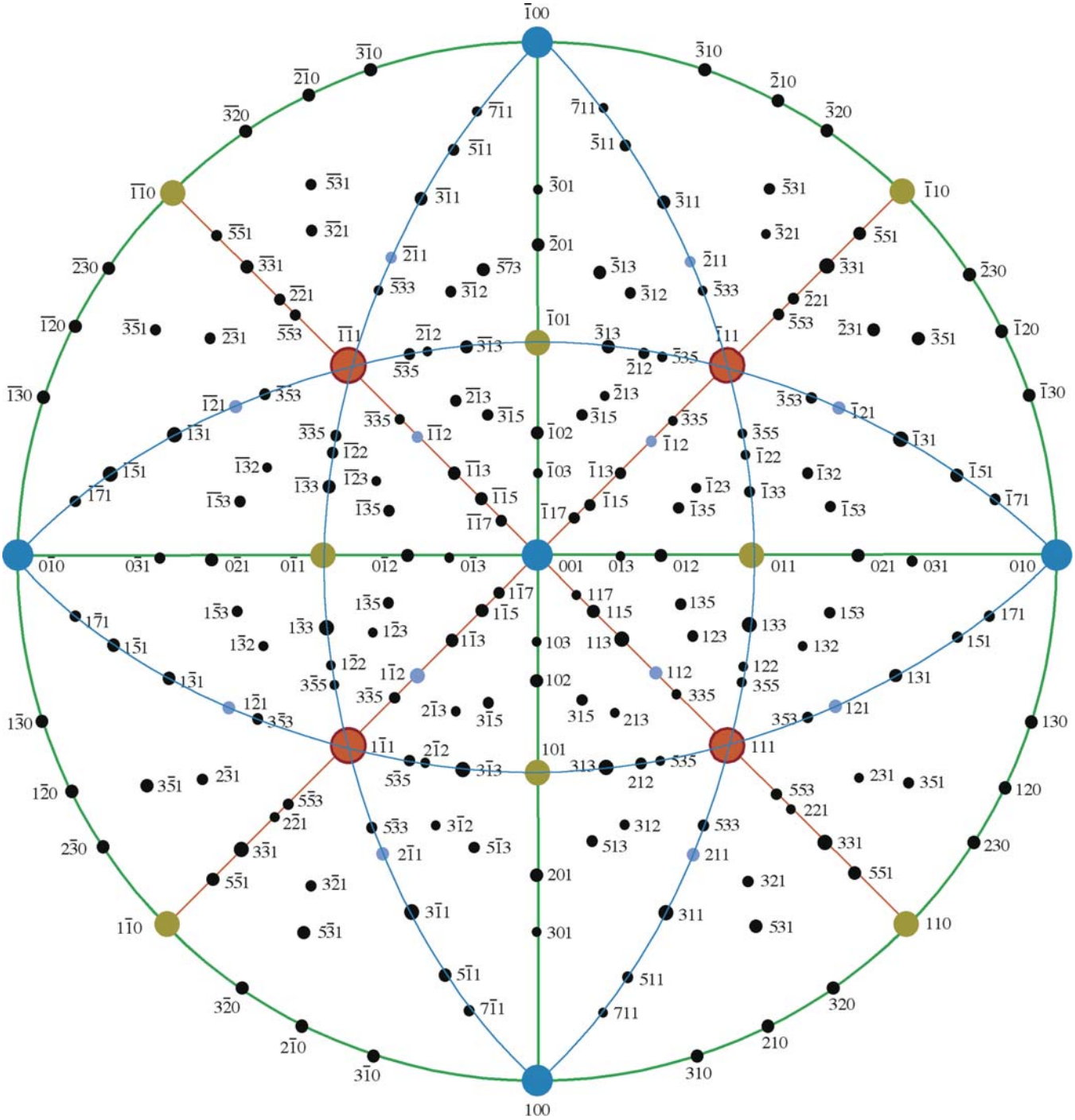

FIGURE 18.5. The stereographic projection for a cubic foil with a [001] normal, assuming the beam is down [001] also. If you want to form an image with the $0\bar{2}2$ reflection, you need to tilt the specimen so the $0\bar{1}1$ pole rotates until it is on the primitive, i.e., it is 90° from the beam direction. To do this, you need to tilt about a pole that is 90° from the $0\bar{2}2$ reflection, such as the [100], [111] or [311] zone axes.

Table 18.1 lists allowed and forbidden reflections for some cubic systems. Rules for more crystal systems are given in Table 16.2.

R AND *d*-SPACINGS

The ratio of any two *R* values gives the inverse ratio of the *d*-spacings.

Once you have tentatively identified possible values for $\mathbf{g}_1$ and $\mathbf{g}_2$, you need to cross-check your answers using the angles between the $\mathbf{g}$ vectors (i.e., the angles between the plane normals). The fully indexed patterns at the end of this chapter (Figures 18.19–18.21) show the principal interplanar angles and the principal ratios of $\mathbf{g}_1/\mathbf{g}_2$. Hence, in practice, you will rarely have to measure more than two or three spacings in order to index a

TABLE 18.1. The Selection Rules for Cubic Crystal Structures

bcc		fcc		Diamond cubic	
$h^2 + k^2 + l^2$	*hkl*	$h^2 + k^2 + l^2$	*hkl*	$h^2 + k^2 + l^2$	*hkl*
2	110				
		3	111	3	111
4	200	4	200	4	200
6	211				
8	220	8	220	8	220
10	310				
		11	331	11	331
12	222	12	222		
14	321				
16	400	16	400	16	400
18	411				
	330				
		19	331	19	331
20	420	20	420		
22	332				
24	422	24	422	24	422
26	431				
		27	511	27	511
		27	333	27	333
30	521				
32	440	32	440	32	440

particular zone-axis DP. However, if your specimen is not oriented close to a zone axis, you'll need to look ahead to Section 18.10.

WEISS ZONE LAW

Check the consistency of your indexing using the Weiss zone law. Each *hkl* reflection must lie in the [*UVW*] zone, i.e., $hU + kV + lW = 0$.

The Weiss zone law only holds for diffraction into the zeroth layer of the reciprocal lattice and the diffraction spots that we see here are called the zero-order Laue zone (ZOLZ). There are circumstances when we can see diffraction from higher-order Laue zones (HOLZ) and we'll talk a lot more about this phenomenon in Chapters 20 and 21. All SADPs, particularly those that we talk about and index in this and the next chapter, are ZOLZ patterns.

The angle between normals to the planes $(h_1k_1l_1)$ and $(h_2k_2l_2)$ is ϕ; the angle between directions $[U_1V_1W_1]$ and $[U_2V_2W_2]$ is ρ. You can work these out and cross-check them with your DPs. These are standard equations in many texts (e.g., those by Edington and Andrews et al.). You'll probably find that the equations for the cubic system are the most useful.

$$\cos\phi = \frac{h_1h_2 + k_1k_2 + l_1l_2}{\left(h_1^2 + k_1^2 + l_1^2\right)^{1/2}\left(h_2^2 + k_2^2 + l_2^2\right)^{1/2}} \qquad (18.3)$$

$$\cos\rho = \frac{U_1U_2 + V_1V_2 + W_1W_2}{\left(U_1^2 + V_1^2 + W_1^2\right)^{1/2}\left(U_2^2 + V_2^2 + W_2^2\right)^{1/2}} \qquad (18.4)$$

Remember that you can always work out these expressions for any crystal system using the equation for the dot product of the two appropriate vectors.

In principle, if we don't know the crystal structure, we can still work out the *d*-spacings of the diffracting planes using equation 18.1. However, you should remember that SAD is not the most accurate method for determining the spacing of lattice planes, d_{hkl}, or the angles between them, ϕ. SAD is generally very good at distinguishing patterns, but it completely fails when the difference between the two patterns is a 180° rotation, as occurs in some patterns of polar material, like GaAs or GaN.

To summarize

- Tilt your specimen to a low-index pole.
- Set $\mathbf{s} = 0$ for the innermost reflections.
- Record the SADP.
- Repeat the exercise using higher-order reflections after tilting the specimen to set $\mathbf{s} = 0$. These measurements will be more accurate, but only if you make sure that $\mathbf{s} = 0$.

The discussion on relrods in Chapter 16 told you that both *d* and ϕ could be seriously in error if reflections are not set to have $\mathbf{s} = 0$, especially since you've probably tilted the specimen.

So far, you have only indexed one DP. You'll probably need more than one to determine orientation relationships. While you're at the microscope, tilt to pole #2 keeping $\mathbf{g}_1$ (see Figure 18.6) strongly excited. Repeat the

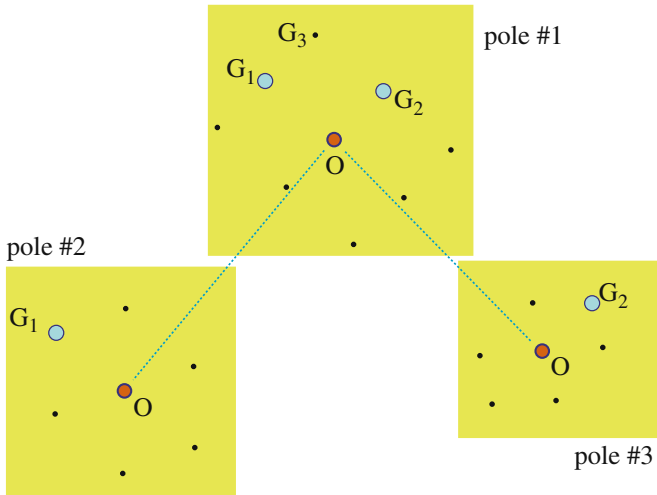

FIGURE 18.6. How to confirm your indexing of reflections and poles by tilting to other poles. Start with $\mathbf{g}_1$ and $\mathbf{g}_2$ strongly excited at pole #1. Tilt to pole #2 keeping $\mathbf{g}_1$ strong, then go back to pole #1 and tilt to pole #3, keeping $\mathbf{g}_2$ strong. Index all the strong reflections each time, measure the tilt angles between each reflection and estimate the tilt between poles.

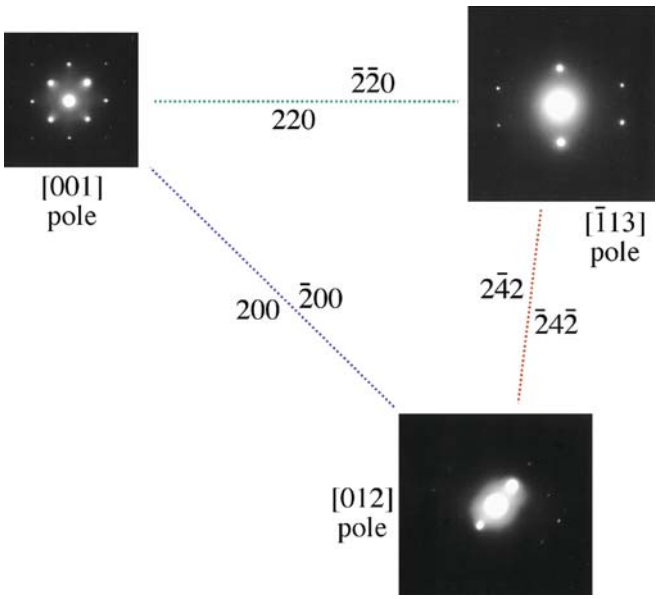

FIGURE 18.7. A practical illustration of the procedure described in Figure 18.6 for an fcc material, in this case MgO.

indexing procedure. Go back to pole #1 and tilt to pole #3 keeping $\mathbf{g}_2$ strongly excited. You can repeat this indexing as many times as you wish. The important idea is that you now have angular measurements allowing you to cross-check your determination of both $\mathbf{g}_1$ and $\mathbf{g}_2$ and the zone axes. Of course the task is simple for an fcc crystal, as you can see in Figure 18.7, which is an experimental illustration of this procedure. The challenge comes when the crystal has less symmetry. If you already know the crystal structure, then you should plot out the most important poles, relating their orientations to one another (more on this in Section 18.11 and Chapter 19) and pay particular attention to the information from systematic absences which occur when the structure factor is zero (go back and check Section 3.9 and Chapter 13).

THE GOLDEN RULE

Make the task as easy as possible. Record *ALL* the DPs you might need and how they relate to one another (draw road maps) while you're at the microscope.

18.5 RING PATTERNS FROM POLYCRYSTALLINE MATERIALS

Diffraction from polycrystalline specimens (especially when the grain sizes are at the nanoscale) can be viewed in much the same way as X-ray diffraction from powders. For a completely random polycrystal, we rotate the reciprocal lattice about all axes and produce a set of nested spheres. When we intersect these spheres with the Ewald sphere (which, in the TEM, approximates to a plane) we will see the rings which are recorded in powder patterns.

NANO AND DPs

Smaller grains give broader spots in the DP. Nanocrystals should give the largest spots, or. . .

If a polycrystal is textured, then there is usually one special plane which is common to nearly all the grains. Since the grains are small, all the reciprocal-lattice points will be broadened by the shape effect; so will the sphere or circles for the polycrystals. This situation will be exacerbated for nanocrystals.

If we then rotate the reciprocal lattice about the lattice vector normal to the texture plane, we produce a set of circles in reciprocal space, as shown in Figure 18.8. If we are examining cubic materials, the reciprocal-lattice vector $\mathbf{g}_{hkl}$ will be parallel to the direction $[hkl]$ in real space. Otherwise this will not generally be the case.

The DP in either of these examples appears as shown in Figure 18.9A and B which differs because the grain

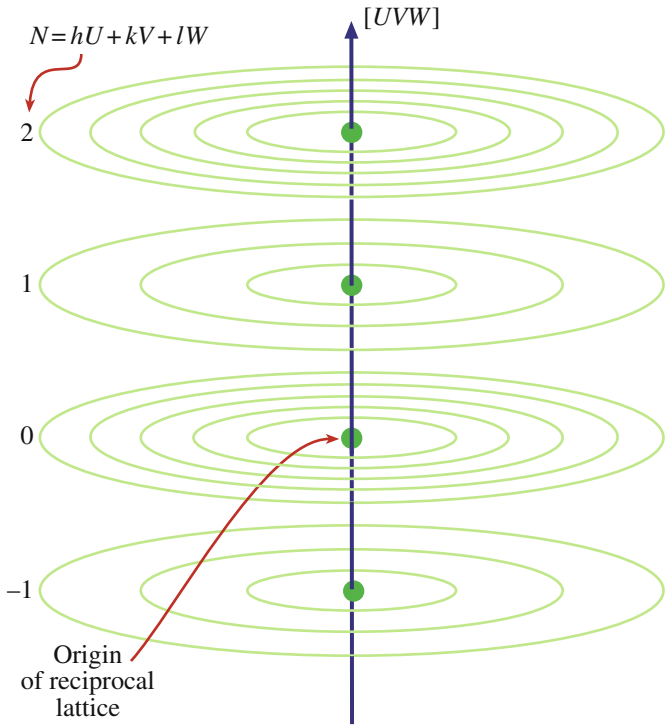

FIGURE 18.8. The generation of a set of circles in reciprocal space by a textured polycrystal. When the reciprocal lattice is rotated about a particular direction $[UVW]$ (in this case the normal to the texture plane) each Laue zone ($N = 1$, 2, etc.) produces a set of concentric circles for each allowed reflection in each zone.

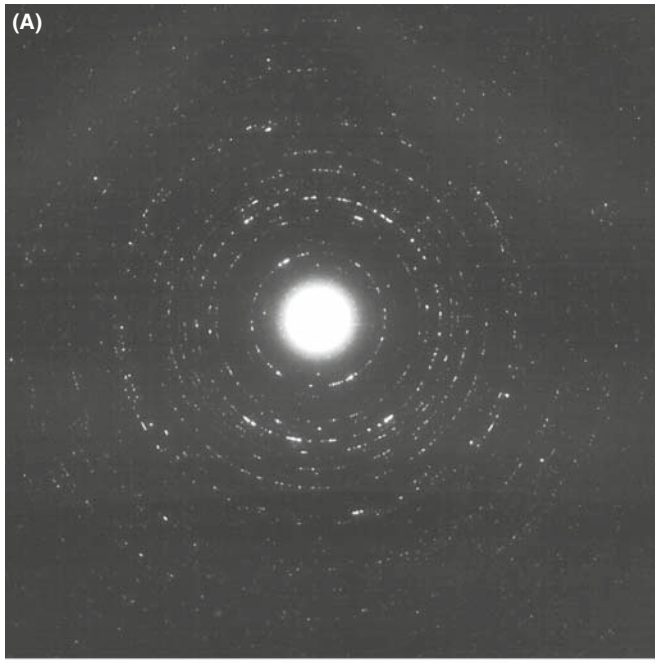

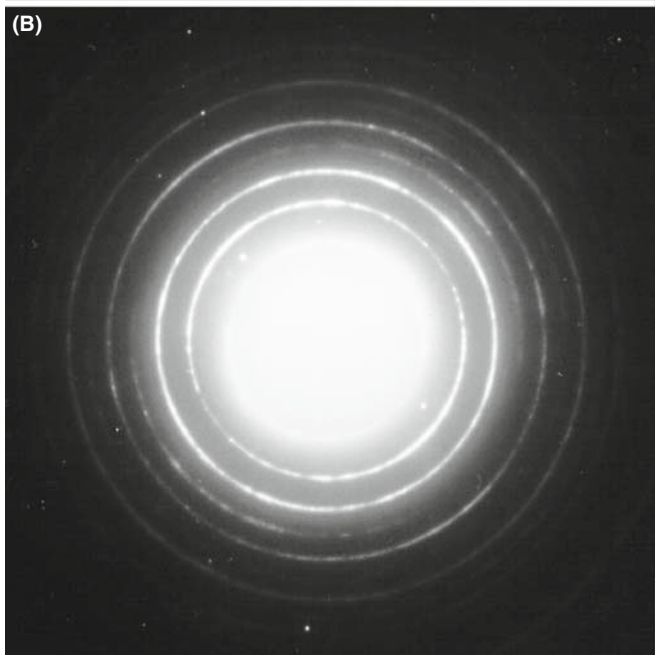

FIGURE 18.9. (A) and (B) Ring DPs from polycrystalline foils. In (A) the grain size is larger than in (B) so the rings are made up of discrete spots. A finer grain size, as in (B) produces a more continuous ring pattern, but the width of the rings of diffracted intensity in fact becomes broader and can be used as an inverse measure of the grain size.

size is different. A larger grain size gives a more speckled pattern.

You can distinguish the pattern produced by a textured specimen from one produced by a random polycrystal by tilting. If your specimen is textured, the rings become arcs as shown in the pattern in Figure 18.10A together with the Ewald-sphere construction in Figure 18.10B. You can locate the grains which give rise to the arcs by forming a CDF image with the arc of diffracted intensity. In Figure 18.10C, these oriented grains are uniformly distributed, but you might encounter a situation where this is not the case. Think how the pattern might differ in this case.

Figure 18.10D and E emphasizes that these ring patterns can be quite varied. In this case the specimen is α-Ag_2Se, which is textured about an axis *inclined* to the beam. When the Ewald sphere cuts the circles now, it produces elongated spots which lie on an ellipse. Vainshtein et al. point out that all the 'spots' on one ellipse can be indexed with the same *hk* indices but a different *l*, and call such a pattern an oblique-textured electron DP. You should also be careful in indexing these textured patterns since not all possible d_{hkl} values need be present, depending on the texture plane.

There is more information in ring patterns than spot patterns. Like a powder pattern, you could estimate the grain size from the width of the rings, but it's more direct (and more reliable) to just look at the DF image. You can see kinematically forbidden rings because you don't necessarily have single scattering from each grain but there are ways around this problem.

Nanocrystalline materials, which fall into our smallest range of ~10-nm grain size, are very challenging because there's probably always more than one grain through the foil thickness. Careful DF imaging combined with HRTEM or CBED with the smallest possible probe (often called nanodiffraction, see Section 21.8.B), is probably optimal, but you need to look for clustering of similarly oriented grains.

18.6 RING PATTERNS FROM HOLLOW-CONE DIFFRACTION

We can combine the advantages of ring patterns from small-grained materials with individual spot patterns from larger-grained materials, As we noted back in Section 9.3.D, if you have a nano/microcrystalline specimen, it is rather inefficient to get a DP from one grain at a time by carefully tilting your specimen and then getting individual DF images of single areas, or of phases within a single grain, by carefully tilting the incident beam. So we can use a computer to continuously change the beam orientation so it samples many angles of incidence and gather DPs from all the crystals superimposed on one another (i.e., get a ring pattern, even from a relatively large-grain material). This is the principle behind hollow-cone (sometimes called 'conical') diffraction (go back and look at Figure 9.15). In the same section we also introduced the idea of hollow-cone DF imaging. In earlier TEMs, before computer control of the beam, hollow-cone illumination was achieved by using an annular C2 aperture rather than a circular hole. Thus the beam that came through the annulus irradiated the specimen from a fixed angle

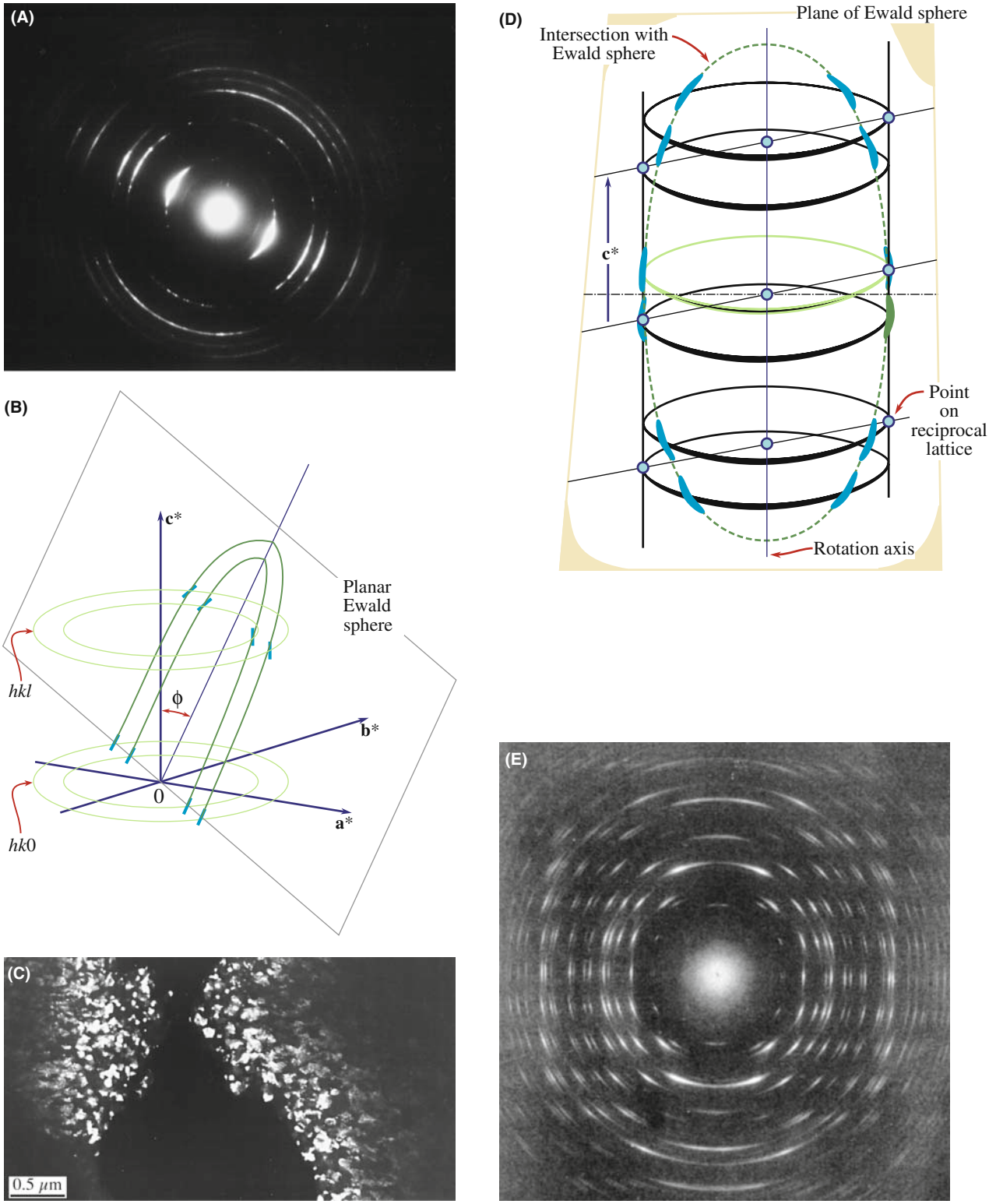

FIGURE 18.10. (A) A textured ring pattern where the rings are more intense over a certain angular range. (B) The corresponding interception of the Ewald sphere (plane) with the reciprocal lattice. (C) A DF image of the textured grains, taken from a brighter potion of one of the *hkl* rings, showing an equiaxed structure. In (D) the specimen is textured about a direction at an angle to the beam, so the Ewald sphere creates elongated spots or arcs in the DP (E).

around the optic axis, as shown schematically back in Figure 9.15A. It's much easier and more flexible to use the computer to control the pre-specimen scan coils and bring the beam onto the specimen at a fixed (or a range of) conical scan angle and a typical conical-scan DP is shown in Figure 9.15B. (If you look ahead, you can see another example of a hollow-cone DF image from an amorphous DP in Figure 18.14C.) Of course, we index the rings in exactly the same way as we described in Section 18.5 for ring patterns obtained from a polycrystalline specimen where the grain size is much smaller than the beam size.

With hollow-cone illumination, we can create a DF image of *all* the crystals in a film that are diffracting from their {*hkl*} planes, rather than imaging only that small fraction diffracting into the part of the diffraction ring that happens to be selected by the aperture. The difference in information content between these two approaches is shown back in Figure 9.15B and C. The hollow-cone technique is widely used in CBED (see Chapter 21) and has more recently been used as the basis for precession diffraction (see Section 18.8.)

18.7 RING PATTERNS FROM AMORPHOUS MATERIALS

Amorphous materials used to represent somewhat of a fringe field in materials science but the rapid growth in glass technology over the last decade, fueled by the optical-communications bubble, the development of bulk metallic glasses and the increased awareness of the role of glassy films at interfaces (particularly the gate oxide in semiconductors) have all conspired to crystallize the following question: *is the material really amorphous or is it (sub) nanocrystalline?* Actually this question is still debated when discussing both amorphous materials and, more intensely, oxide and metallic glasses because there's still no broadly accepted definition of when grains become small enough that a determinable crystal structure no longer exists. At best we should think of a continuum of states from nanocrystalline to amorphous.

DPs AND AMORPHOUS MATERIALS
The DP from an amorphous material looks similar to that from polycrystalline material but the rings are broader and there is no speckle.

Rudee and Howie showed that electron scattering from regions of $\leq$1.5 nm diameter could be coherent. Graczyk and Chaudhari proposed modeling these materials as random networks. If we are careful, we can learn quite a lot about the structure of amorphous materials, but we should first say what we mean by 'amorphous.'

> An amorphous material is one where the locations of the neighboring atoms are defined by a probability function such that the probabilities are never unity.

This idea is best illustrated by a plot of the probability which we call the *radial distribution function* (RDF). The RDF, $\rho(r)$, is the probability, per unit element of volume, that an atom will be found at a distance r from another atom. The first example in Figure 18.11A compares the curves for liquid sodium and crystalline sodium; the numbers on the crystalline curve remind us that in the crystal each sodium has eight nearest neighbors, etc. The second plot, Figure 18.11B, shows the RDF for vitreous silica. This time the peaks are associated with distances

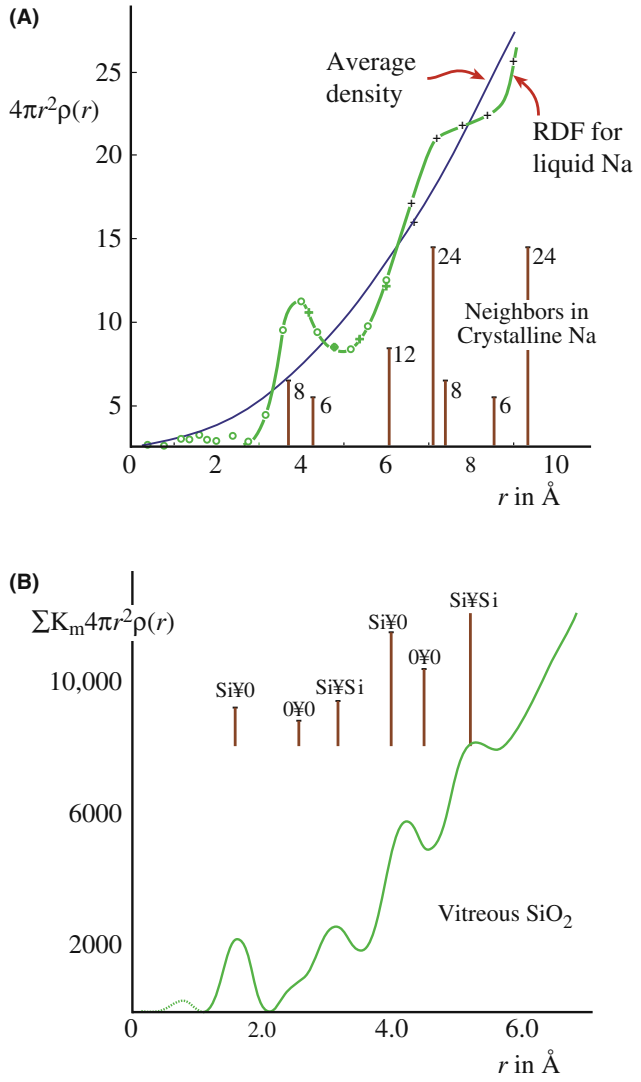

FIGURE 18.11. (A) Radial distribution functions for liquid Na and the average density curve superimposed on the distribution of the nearest neighbors in crystalline Na (vertical lines). (B) The RDF for vitreous SiO_2 is peaked at a distance that represents spacings between Si and O atoms.

between different pairs of Si and O atoms. The features to notice are

- The two curves both show definite peaks.
- The two curves are different.

Some diffraction theory. Since these materials are so different, we'll give a brief introduction to the theory of scattering from amorphous materials. We make the assumption that the electron beam is only scattered once; this is kinematical, but it's more realistic than for crystals at the Bragg condition. Following Howie, we express the kinematical intensity, $I(\mathbf{k})$, by the expression

$$I(\mathbf{k}) = |f(\mathbf{k})|^2 \sum_{i,j} e^{i2\pi\mathbf{k}.(\mathbf{r}_i - \mathbf{r}_j)} \tag{18.5}$$

Here we assume that there are N identical atoms contributing to the scattered intensity and they are located at the different positions ($\mathbf{r}_i$ or $\mathbf{r}_j$).

The $f(\mathbf{k})$ terms are the atomic scattering amplitudes, with $\mathbf{k}$ reminding us that there is an angular dependence to f. If the material is isotropic, we can simplify equation 18.5 as follows

$$I(\mathbf{k}) = N|f(\mathbf{k})|^2 \left(1 + \frac{F(\mathbf{k})}{k}\right) \tag{18.6}$$

where

$$F(\mathbf{k}) = \sum_{i \neq j} e^{i2\pi\mathbf{k}.(\mathbf{r}_i - \mathbf{r}_j)} \tag{18.7}$$

$$F(\mathbf{k}) = k \int \rho(r) e^{i2\pi\mathbf{k}.\mathbf{r}} dV \tag{18.8}$$

$$F(\mathbf{k}) = 4\pi \int_0^\infty \rho(r) \sin(2\pi k r)\, r\, dr \tag{18.9}$$

The term $\rho(\mathbf{r})$ is the RDF. Equation 18.9 can be inverted to give an expression for ρ

$$\rho(\mathbf{r}) - \rho_0 = \frac{1}{r} \int_0^\infty F(\mathbf{k}) \sin 2\pi k r\, dk \tag{18.10}$$

This equation means that, in principle, the RDF can be obtained directly from DPs. This process is enhanced if the patterns are energy-filtered to remove inelastic contributions (see Chapter 37 and the work of Cockayne et al.) as shown graphically in Figures 18.12 and 18.13. Compare these figures with Figure 2.13A. Other ways to determine the RDF include extended X-ray absorption fine structure (EXAFS) studies in a synchrotron X-ray and, less expensively but more noisily, via EXELFS (see Chapter 40). Alternatively, we can rearrange equation 18.6 again to give a 'reduced-intensity function' as illustrated by the work of Graczyk and Chaudhari who

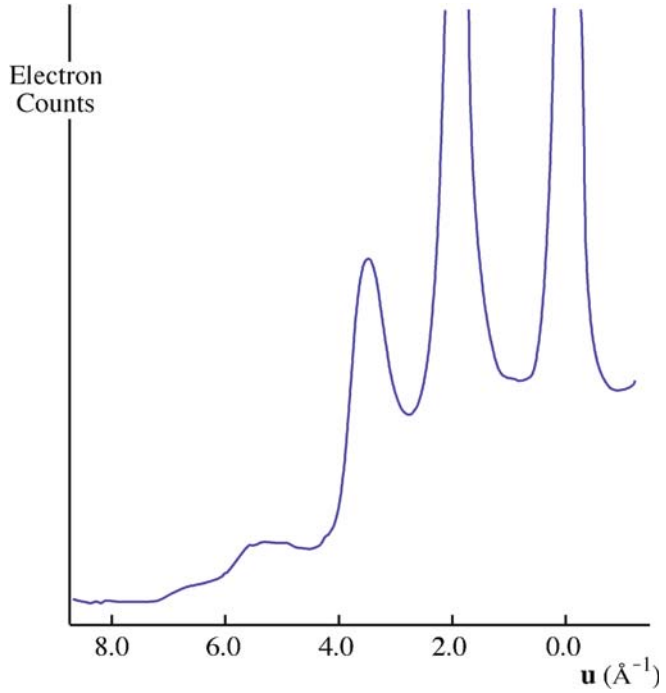

FIGURE 18.12. An intensity profile across an energy-filtered DP from amorphous Si obtained by scanning the pattern across the entrance slit to a serial EELS spectrometer and recording only the elastic (on-axis) electrons.

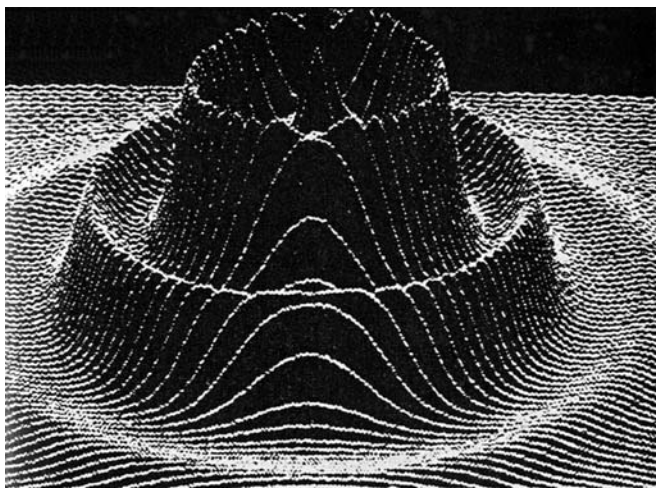

FIGURE 18.13. A computer plot of the diffracted intensity distribution from an amorphous structure, showing diffuse rings of intensity. The direct-beam intensity is off-scale.

showed clearly that the structure correlation can extend to 1.5 nm or more. Life gets more interesting as we explore the structure out beyond the nanometer level and Treacy et al. review a new imaging technique called fluctuation microscopy which is a hybrid imaging/diffraction technique sensitive to the presence of medium-range order in amorphous materials. We'll discuss this technique more in Chapter 29. If you get the idea that

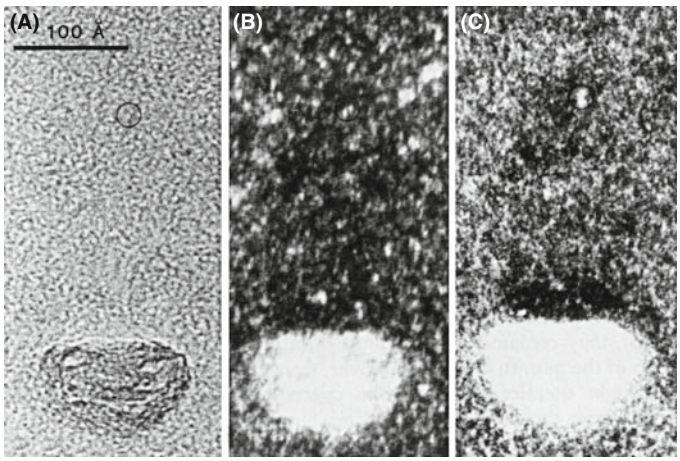

FIGURE 18.14. (A) BF image of amorphous carbon. (B) DF image from the diffuse diffracted intensity taken with a defocused beam and (C) hollow-cone image showing more structure.

the study of amorphous materials is at the frontiers of TEM materials-structure determination, you are right!

To summarize this discussion, the scattering theory is well known but the capability for routinely removing the inelastic contribution is only now becoming available and is still not commonplace. Probably the best way to answer whether a material is nanocrystalline or amorphous will come from a combination of SAD and EELS. A BF image of amorphous material is generally uninformative (Figure 18.14A), but if you try to form a DF image you will see a speckle of white spots against a dark background, as shown in Figure 18.14B. The size of the speckle increases as the defocus increases, so be wary of interpreting the image in terms of the size of regions in the amorphous structure. Hollow-cone DF imaging, as shown in Figure 18.14C, gives even more and finer 'structure' in the image. The fact that you can produce this type of speckled contrast is important because you may well want to study small particles (e.g., catalysts) supported by an amorphous film. In such a case, you need to know what the image of the support film looks like before you add a new component.

Glass at interfaces and grain boundaries. Another area where it is important to know whether or not an amorphous material is present, occurs in the analysis of grain boundaries in ceramic materials or gate oxides in semiconductor devices. Answering this problem severely taxes the limits of HRTEM when the film thicknesses are < 1 nm, which is the case for the gate oxide in the latest semiconductor devices. For somewhat thicker films we can use conventional HRTEM and another technique, known as diffuse-dark-field (DDF) imaging, which essentially forms an image from the region in the SADP where the amorphous ring would be, if glass were present. We'll return to DDF imaging in Chapter 29.

18.8 PRECESSION DIFFRACTION

Precession is a relatively new approach to performing electron diffraction; it is similar to the X-ray method which goes by the same 'name' (although in XRD the crystal, rather than the beam, is precessed) and it is closely related to hollow-cone diffraction that we just talked about. The main advantage that precession brings is to remove strong dynamical effects from the patterns leaving high-quality kinematical data, eliminating, e.g., extra spots due to dynamical effects. Precession diffraction can also be used for crystal structure and full symmetry determination. While the method was first tried in a TEM by Vincent and Midgley, recent advances in both CCD cameras and (you've guessed it) aberration correction make both the operational aspects and the interpretation of precession DPs much easier.

In precession diffraction we double-deflect the incident beam (either parallel or convergent) using the usual DF scan coils in a circular hollow cone (radius G and angle C) about a centered zone-axis direction (Figure 18.15) and de-scan the beam onto the plane of the DP. So it is really a double conical beam-rocking system.

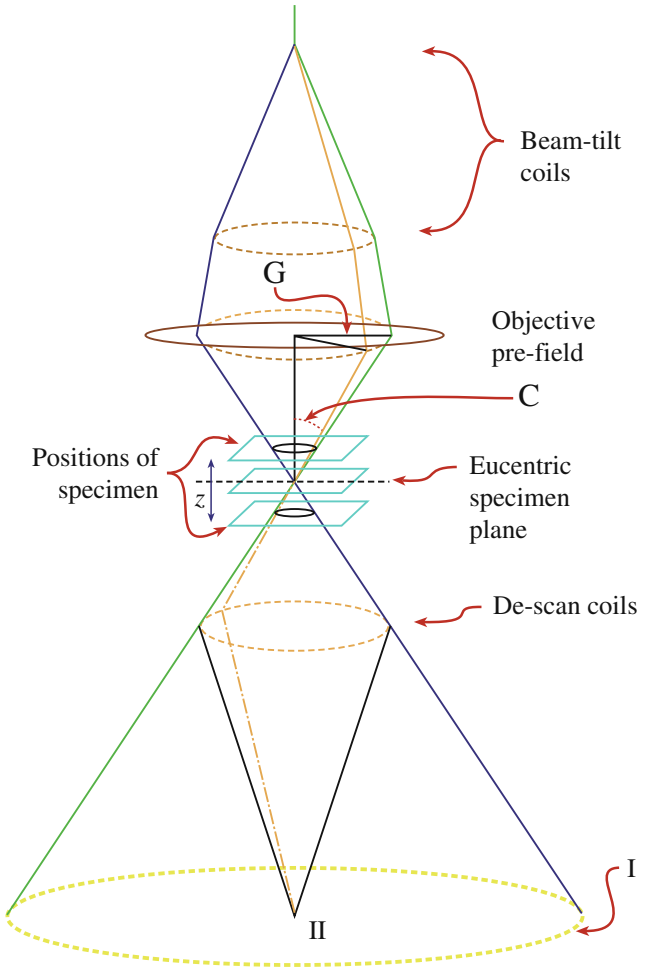

FIGURE 18.15. Schematic ray diagram for precession diffraction.

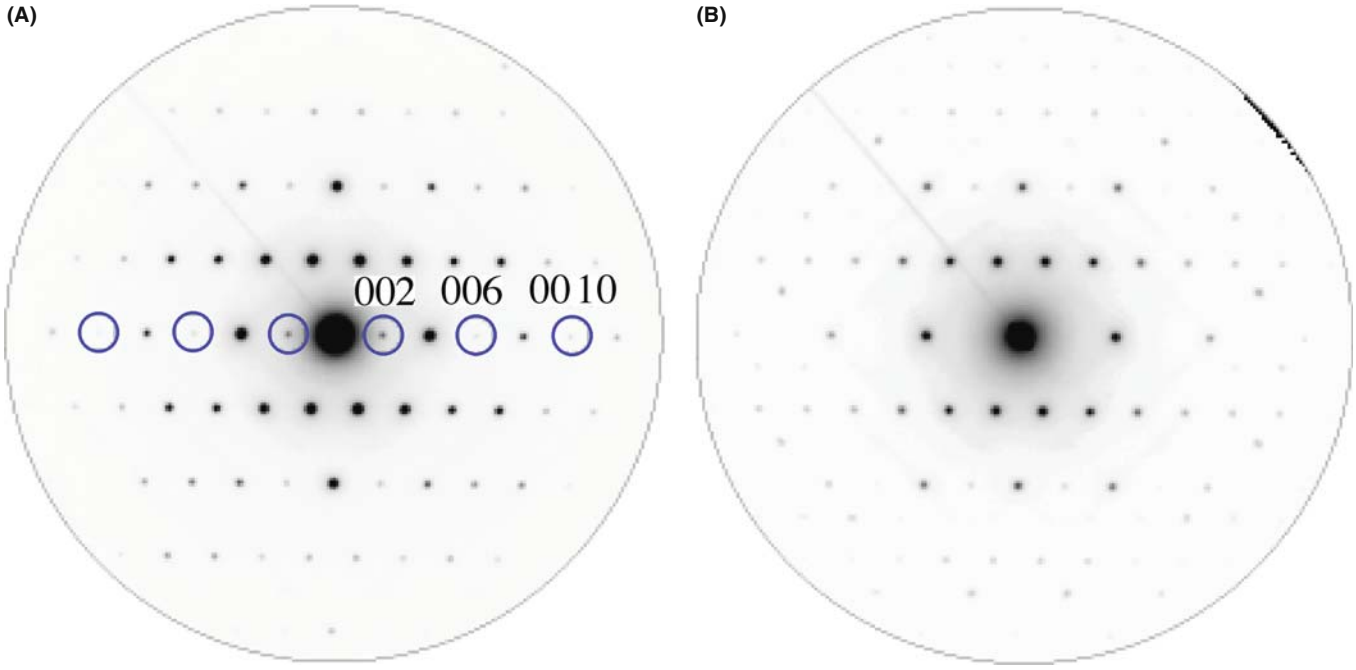

FIGURE 18.16. Si <130> DP taken (A) with a small precession angle (1°) and (B) with a large precession angle (3°). The kinematically forbidden reflections 002, 006, 0010 disappear at the larger precession angle. Note also the appearance of strong differences in the intensity of individual *hkl* maxima.

Unlike standard TEM hollow-cone where we are seeking to get multiple (i.e., ring) patterns sampling many grains, in precession mode we are usually trying to average out the diffraction conditions within a single grain and obtain a single-crystal pattern in which dynamical effects are reduced. If the hollow-cone angle is large enough, all the diffraction data correspond to a two-beam condition and show reduced dynamical diffraction because not many reflections are simultaneously excited off the zone-axis condition. When we precess the beam, we integrate the diffracted intensities through the Bragg condition, so small specimen-tilt changes are averaged out and we can more reliably interpret crystal-symmetry information in the DP. Continuous changing of the precession angle over several degrees can help with point and space-group determination (see Chapter 21, the companion text and Morniroli et al.'s paper). Figure 18.16A and B shows, respectively, the differences between small and large precession-angle DPs from a Si single crystal. The larger angle removes the kinematically forbidden reflections that are present in the smaller-angle DP because the multiple-diffraction paths to them are unlikely to occur during the precession movement. Most of the time, only the direct beam and one diffracted beam are strongly excited as the beam precesses. This does not mean that the dynamical interactions disappear, they just occur between the direct beam and one diffracted beam (as in the two-beam case).

Precession is an area of electron diffraction that is seeing a rapid growth in applications across many fields. Commercial retrofits are available for any TEM (e.g., URL #3) but, if you want to do it on your own, then Own et al. give good detailed instructions.

18.9 DOUBLE DIFFRACTION

Double diffraction occurs when a diffracted beam traveling through a crystal is rediffracted either within the same crystal or when it passes into a second crystal. If the initial diffraction vector of the beam is $\mathbf{g}_1$ and it is rediffracted by reflection $\bar{\mathbf{g}}_2$, then the resultant diffraction vector of the double-diffracted beam is $(\mathbf{g}_1 - \mathbf{g}_2)$. If $\mathbf{g}_2$ is not an allowed reflection in the first crystal, the double-diffracted beam is characteristic of neither the first nor the second crystal.

Reflections attributable to double diffraction are a common feature of DPs recorded from two-phase materials exhibiting epitaxy or topotaxy including, e.g., oxidized metallic specimens. Quite complicated patterns may be formed, requiring careful analysis to distinguish the 'real' reflections from the double-diffraction reflections. Double diffraction is directly responsible for the moiré effect in the electron images that we will discuss in Chapter 23. As an example of this effect, we'll consider small α-Fe_2O_3 (hematite) islands grown on a single-crystal α-Al_2O_3 (alumina or sapphire) substrate as

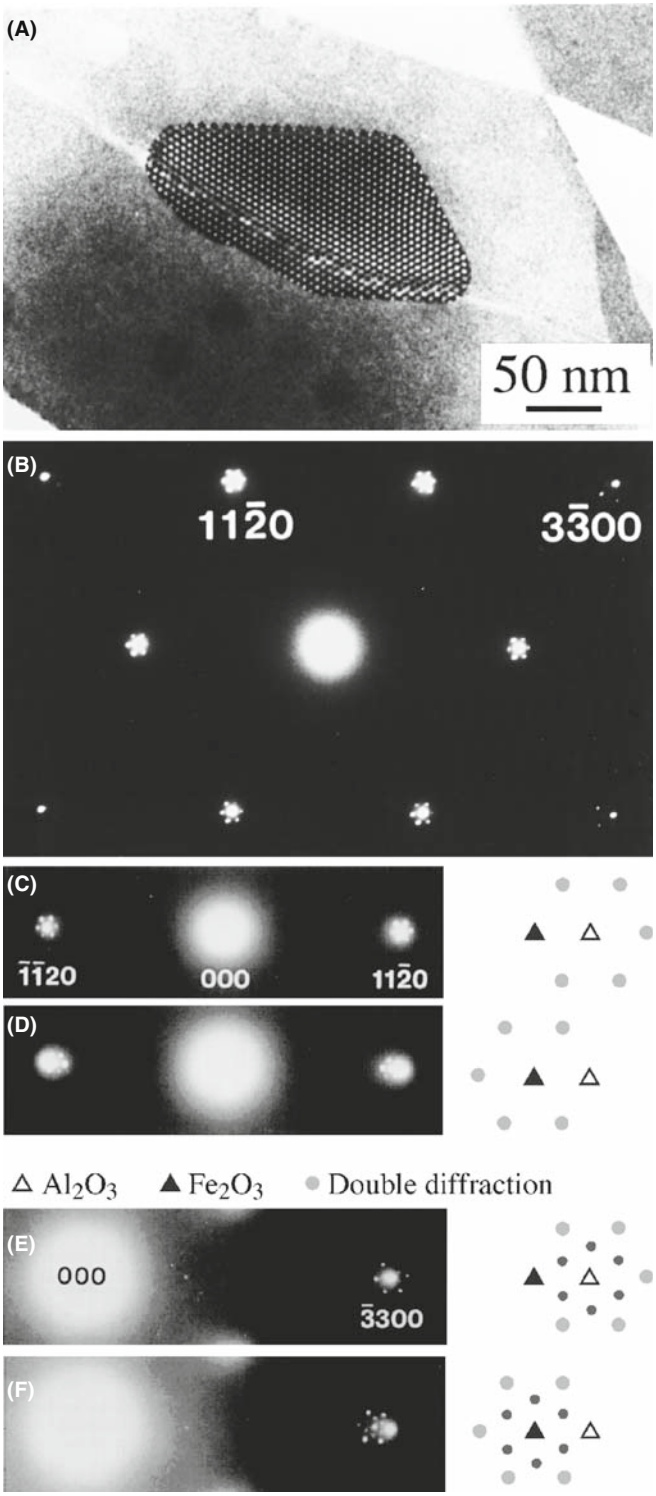

FIGURE 18.17 (A) BF on-axis image of a particle of α-Fe_2O_3 on α-Al_2O_3. (B) [0001} SADP from α-Fe_2O_3 showing double-diffraction spots around the $\{11\bar{2}0\}$ and $\{3\bar{3}00\}$ reflections. (C) Enlargements of regions near the $\{11\bar{2}0\}$ reflections when the hematite island is on the top surface. (D) Enlargements of regions near the $\{11\bar{2}0\}$ reflections when the hematite island is on the bottom. (E) Enlargements of regions near the $\{3\bar{3}00\}$ reflections when the hematite island is on the top surface. (F) Enlargements of regions near the $\{3\bar{3}00\}$ reflections when the hematite island is on the bottom.

shown in Figure 18.17A. The position of the double-diffraction spots relative to the hematite and alumina reflections actually changes depending on whether the islands were on the top or bottom surface of the specimen. This particular top–bottom effect can be derived from simple geometry; however, dynamical diffraction effects must also be considered when the materials are thicker.

Figure 18.17B shows the [0001] SADP recorded from one of these α-Fe_2O_3 particles. The closest reflections to the direct beam are the six $\{11\bar{2}0\}$ reflections. The next closest reflections are the six $\{3\bar{3}00\}$ reflections, only four of which are visible in the figure. Double-diffraction spots are visible around each of these primary reflections. They also surround the direct beam, although they are hidden by the flare from that beam in Figure 18.17B.

Figure 18.17C and D shows enlargements of regions near the $\{11\bar{2}0\}$ reflections in the [0001] SADPs recorded when the hematite island was on the top surface in (C) and on the bottom surface of the sapphire in (D). Both $\mathbf{g}$ and $\bar{\mathbf{g}}$ reflections are shown for the two cases. In (C) the ring of six double-diffraction spots surrounds the Al_2O_3 reflection while in (D) the double-diffraction spots surround the Fe_2O_3 reflection.

The same observation can be made for the $\{\bar{3}300\}$ regions of the SADPs as shown in Figure 18.17E and F. In this case, an inner ring of double-diffraction spots (small filled circles) with the same spacing and orientation as the double-diffraction reflections in Figure 18.17C and D are still visible, as are the outer rings of spots (large filled circles). In general, the outer ring of double-diffraction spots is more intense than the inner ring.

This top-bottom effect in particular, and double diffraction in general, can be explained by the simple geometric analysis we show in Figure 18.18; the bottom crystal is Al_2O_3, which has the smaller lattice parameter and therefore has the larger reciprocal-lattice vectors. Double-diffraction spots can be formed around the primary hematite reflection, $\mathbf{g}_H$, by two different routes

- $2\mathbf{g}_H + \bar{\mathbf{g}}_A$ (A: alumina, H: hematite) giving the double-diffraction spot just inside $\mathbf{g}_H$.
- $\bar{\mathbf{g}}_H + 2\mathbf{g}_A$ gives a double-diffraction spot just outside $\mathbf{g}_H$.

These two routes at first appear to be equivalent. However, if we take into account the curvature of the Ewald sphere, then the deviation parameters of the two routes are very different. In the case of diffraction through the upper crystal, the deviation parameter of the $2\mathbf{g}$ beam is slightly more than twice that of the $\bar{\mathbf{g}}$ beam. This difference will not significantly affect the intensities from a very

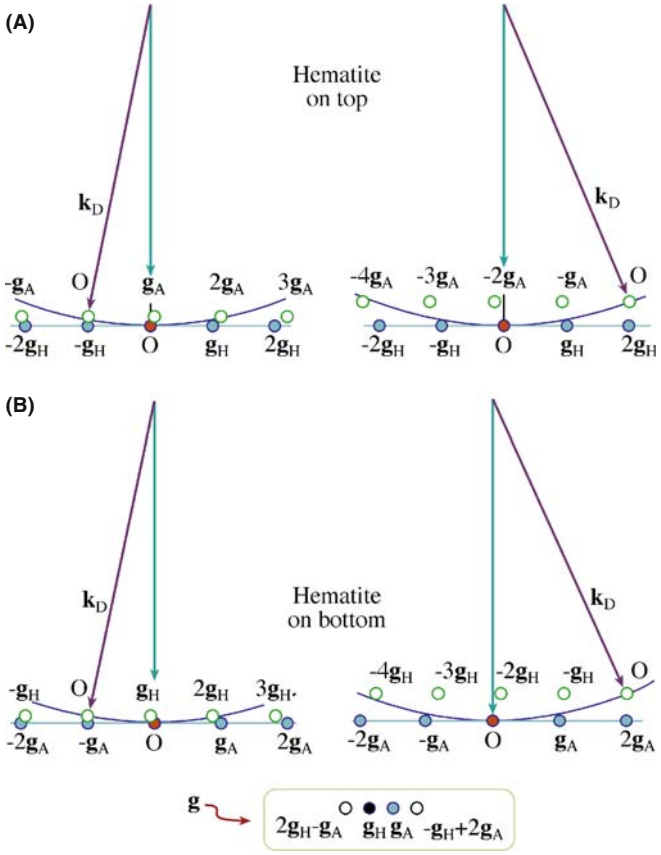

FIGURE 18.18. Top-bottom effect in double diffraction. The pattern depends on which of the two crystals is on top. In this case α-Fe_2O_3 particles are on top of the Al_2O_3 and the two (non-equivalent) paths (A) and (B) for double diffraction are shown. NOTE: $\mathbf{g}_A$ is for alumina and $\mathbf{g}_H$ for hematite.

thin epilayer due to streaking of the reciprocal-lattice spots parallel to the beam direction (the shape-factor effect).

Now we can analyze the effects of diffraction through the lower crystal

- Draw the reciprocal lattice with the origin of the Ewald sphere at $2\mathbf{g}_H$ for the first case and on $\bar{\mathbf{g}}_H$ in the second.
- Keep the radius of the Ewald sphere unchanged since only elastic interactions are considered.
- The incident beam for the lower crystal is in the $2\mathbf{g}$ or $\bar{\mathbf{g}}$ directions for the two cases.
- The height of the ZOLZ is slightly different in the two cases since the deviation parameter at the origin must be zero.

You can see from Figure 18.18A that the deviation parameter for $2\mathbf{g}_A$ is approximately zero, whereas for $\bar{\mathbf{g}}_A$ it is of the same order as $\mathbf{g}_H$. The total deviation parameter is thus much smaller for the second route than the first. A similar analysis for the inverted structure is shown in Figure 18.18B. In both cases, the deviation parameter for the route $\bar{\mathbf{g}}$ (upper) plus $2\mathbf{g}$ (lower) produces a much smaller deviation parameter than the route $2\mathbf{g}$ (upper) plus $\bar{\mathbf{g}}$ (lower). So the double-diffraction spot, which occurs on the same side of the diffraction spot from the upper crystal as the diffraction spot from the lower crystal, will be more intensely excited than the double-diffraction spot which occurs on the opposite side. In two dimensions, for thin films, the strongest double-diffraction spots will always be those arranged symmetrically around the diffraction spot from the lower crystal.

For thicker layers, the relative intensity of the $\bar{\mathbf{g}}$ and $2\mathbf{g}$ beams will vary as dynamical diffraction effects occur. We can simulate the DPs from these structures using the MacTempas program (see Chapter 30 and Section 1.6.B) The top-bottom effect is evident in the case of 2.7 nm of hematite on 13 nm of alumina, but only just discernible for the case of 2.6 nm of alumina on 13.5 nm of hematite. In the latter case, the dynamical diffraction effects are stronger.

We will meet this topic in Chapter 23 when we discuss moiré fringes. We have made this analysis a little more complicated than usual since we have considered the details of where the spots will actually be found. You can make this process simpler

- Trace the patterns from each crystal (if you know what tracing paper is).
- Then construct a new pattern using each diffracted beam from the upper crystal as an incident beam for the lower crystal.

The extent of the moiré pattern gives you an idea of just how strong dynamical scattering is, even for thin films!

18.10 ORIENTATION OF THE SPECIMEN

Once you have identified three $\mathbf{g}$ vectors $\mathbf{g}_1$, $\mathbf{g}_2$ and $\mathbf{g}_3$ in a single-crystal DP, you can calculate the direction of the beam $\mathbf{B}$. You can actually estimate $\mathbf{B}$ to within about 10° from the vector cross product as follows

$$\mathbf{B} = \mathbf{g}_1 \times \mathbf{g}_2 = \begin{bmatrix} \mathbf{i}_1 & \mathbf{i}_2 & \mathbf{i}_3 \\ h_1 & k_1 & l_1 \\ h_2 & k_2 & l_2 \end{bmatrix} \tag{18.11}$$

$$= (k_1 l_2 - k_2 l_1, l_1 h_2 - l_2 h_1, h_1 k_2 - h_2 k_1) \tag{18.12}$$

For the three-beam case, you can determine $\mathbf{B}$ with an accuracy of $\sim 3^\circ$. You first need to make sure that the three vectors are taken in the correct order. Draw a circle through these three reflections: if O is inside the circle, then the $\mathbf{g}$ vectors should be numbered counterclockwise; if O is outside, number them clockwise. Check your labeling; the determinant of the matrix in equation 18.13 should be positive

$$\mathbf{g}_1 \cdot (\mathbf{g}_2 \times \mathbf{g}_3) = \frac{1}{V} \begin{bmatrix} h_1 & k_1 & l_1 \\ h_2 & k_2 & l_2 \\ h_3 & k_3 & l_3 \end{bmatrix} \tag{18.13}$$

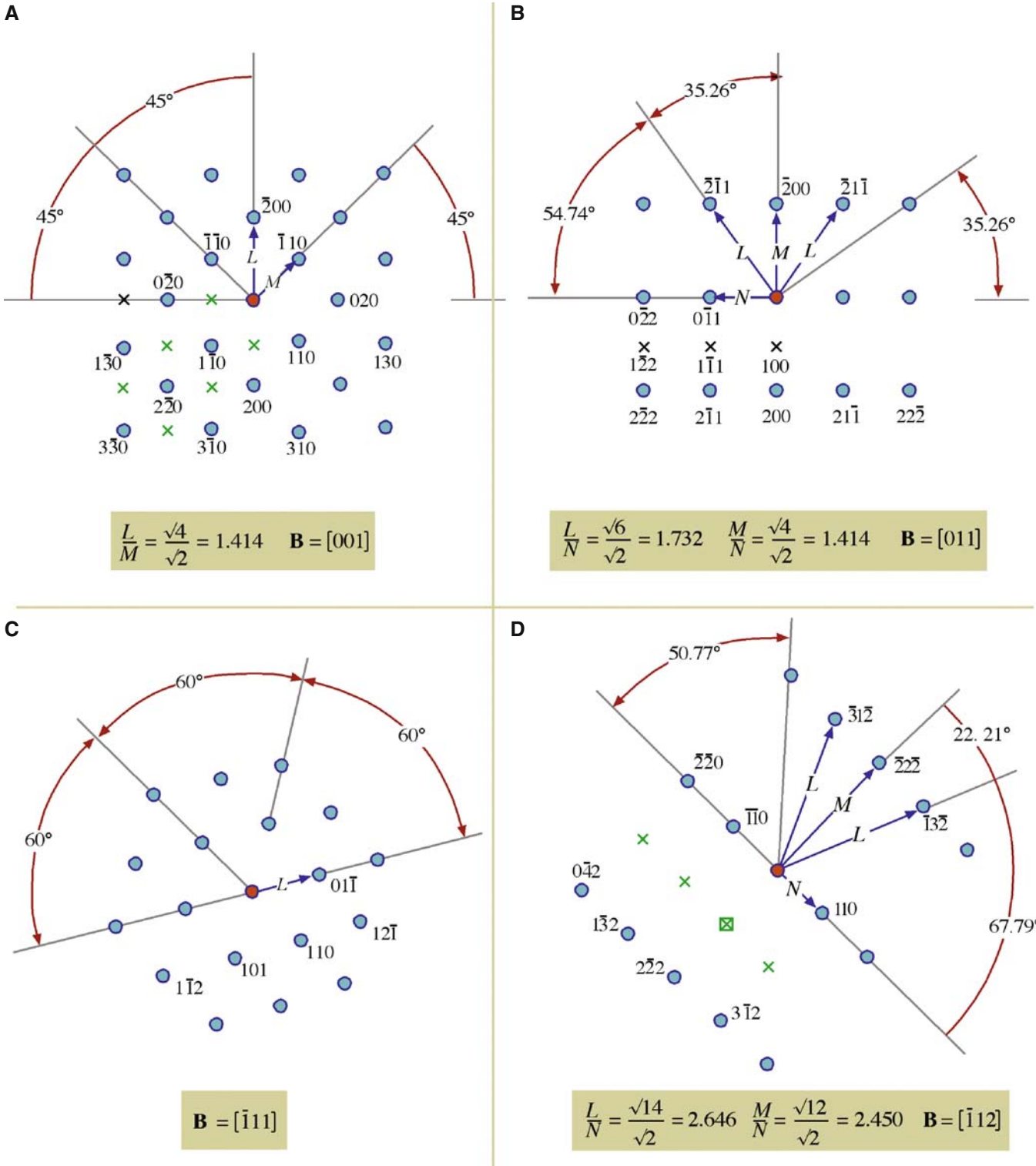

FIGURES 18.19. Four standard, indexed, DPs for bcc crystals in the [001], [011], $[\bar{1}11]$ and $[\bar{1}12]$ beam directions. Ratios of the principal spot spacings are shown as well as the angles between the principal plane normals. Forbidden reflections are indicated by x.

Now we can write a weighted-average expression for **B**

$$\mathbf{B} = \frac{\mathbf{g}_2 \times \mathbf{g}_3}{|\mathbf{g}_1|^2} + \frac{\mathbf{g}_3 \times \mathbf{g}_1}{|\mathbf{g}_2|^2} + \frac{\mathbf{g}_1 \times \mathbf{g}_3}{|\mathbf{g}_3|^2} \qquad (18.14)$$

OUR CONVENTION

The vector **B** points up the column. It is normal to the emulsion side of a photographic negative. The electron beam travels along the direction –**B.**

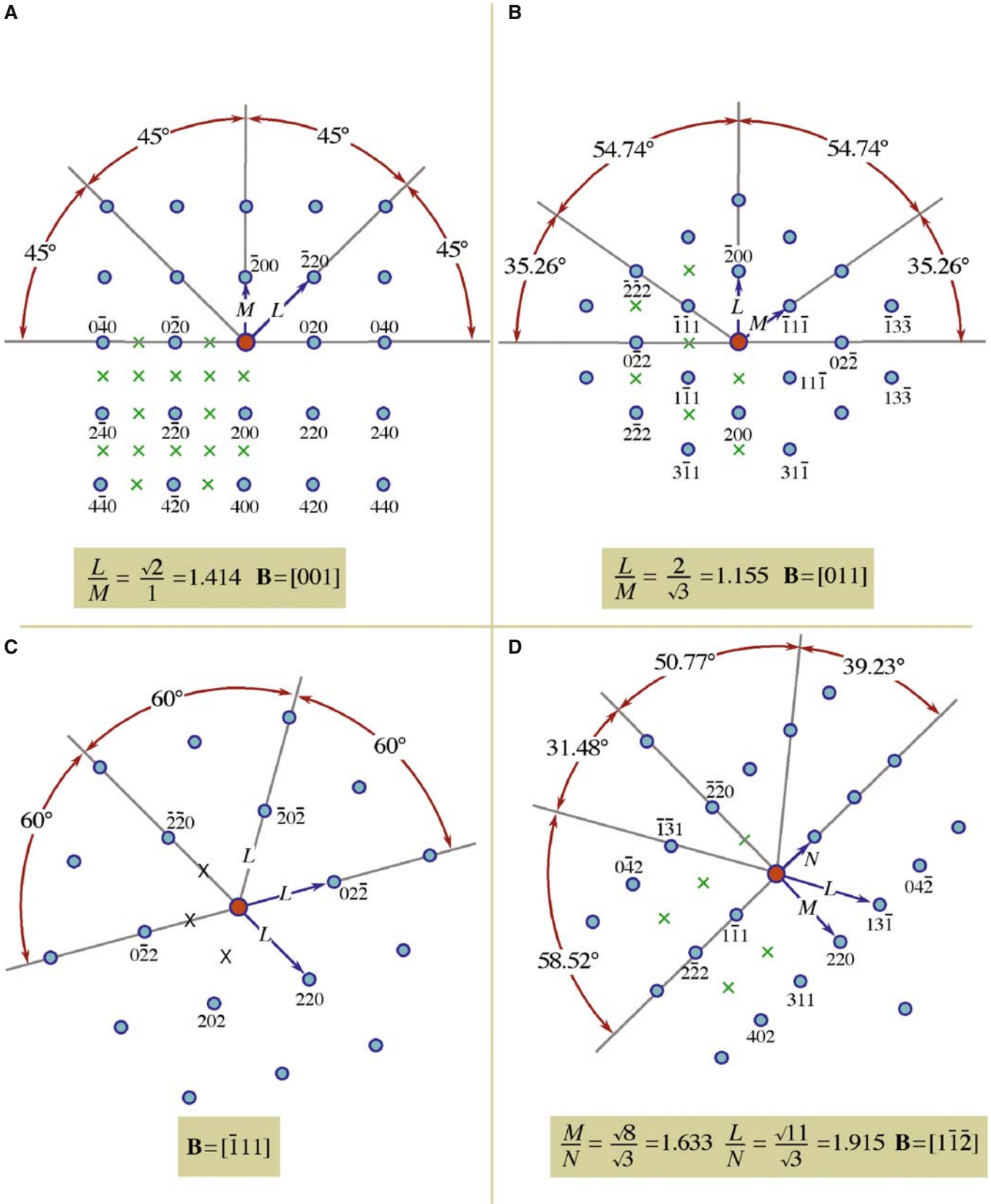

FIGURES 18.20. Four standard, indexed, DPs for fcc crystals in the [001], [011], [$\bar{1}$11] and [$\bar{1}$12] beam directions. Ratios of the principal spot spacings are shown as well as the angles between the principal plane normals. Forbidden reflections are indicated by x.

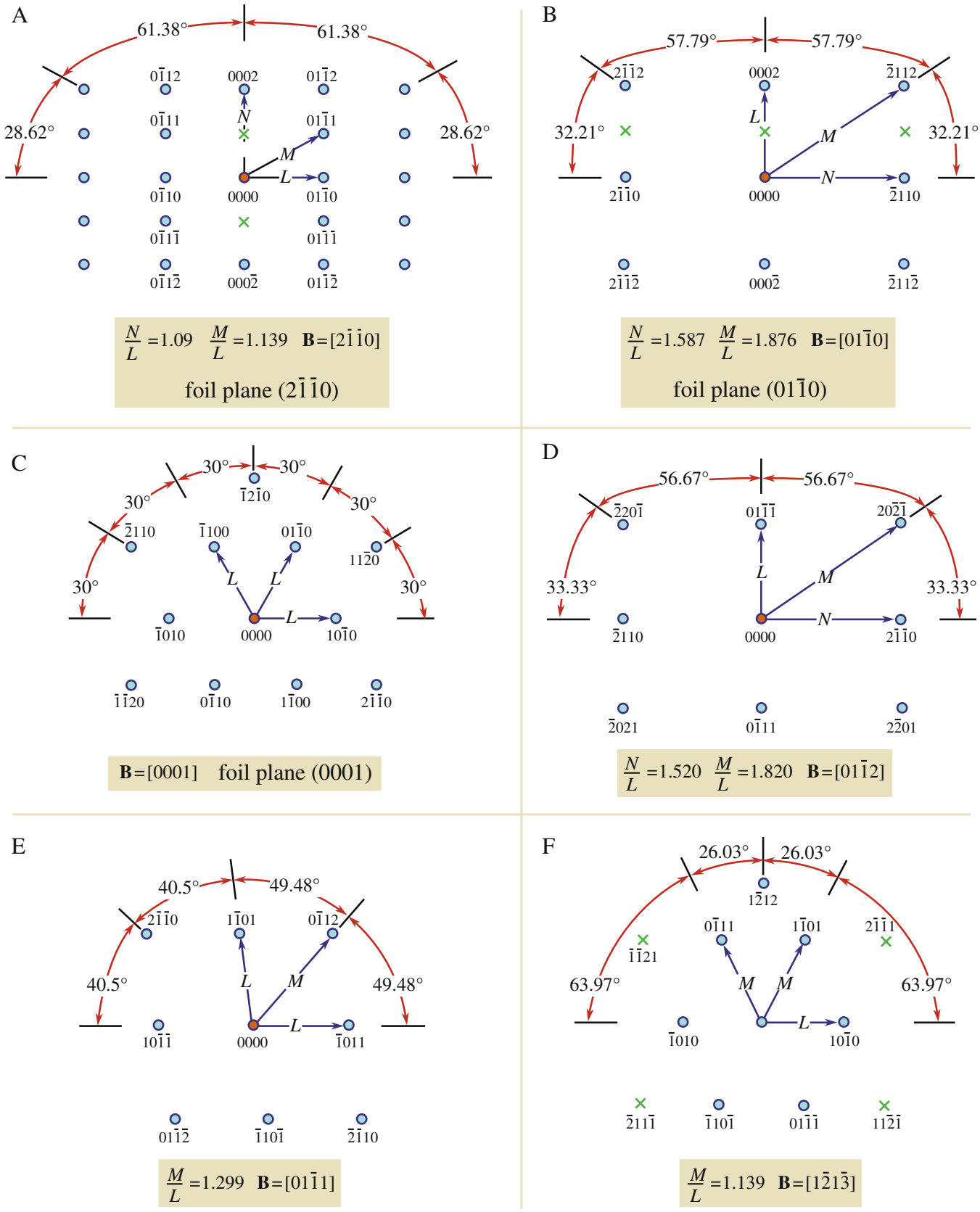

FIGURES 18.21. Six standard, indexed, DPs for hcp crystals in the [$2\bar{1}\bar{1}0$], [$01\bar{1}0$], [0001], [$01\bar{1}2$], [$01\bar{1}1$] and [$1\bar{2}1\bar{3}$] beam directions. Ratios of the principal spot spacings are shown as well as the angles between the principal plane normals. Forbidden reflections are indicated by x.

In Figures 18.19–18.21, we illustrate some of the most useful DPs for bcc, fcc and hcp crystals. You can extend these patterns as far as you wish using vector addition; remember the reflections correspond to reciprocal-lattice *vectors*. For example, in Figure 18.19C

$$(12\bar{1}) = (110) + (01\bar{1}) \qquad (18.15)$$

You can extend the patterns in this way and then apply the selection rules to find the corresponding patterns for Si, etc., using the specific examples as a guide.

- bcc real space —> fcc reciprocal space.
- fcc real space —> bcc reciprocal space.

Take the example used by Edington, as shown in Figure 18.22 for an fcc crystal. Measure the distances to the reflections x, y and z. Since the material is fcc, we can ratio d^2 values to find suitable indices or use a calibrated camera length. Thus we find that plane $A = (4\bar{2}0)$, $B = (111)$ and $C = (\bar{3}31)$; check that the angles are correct using

$$\cos(\phi_{AB}) = \frac{\mathbf{g}_A \cdot \mathbf{g}_B}{|\mathbf{g}_A||\mathbf{g}_B|} \qquad (18.16)$$

and so on for ϕ_{BC} and ϕ_{CA}. You should immediately recognize that this is the $\pm[12\bar{3}]$ pole, but continue. Now you can plug pairs of these indices into equation 18.11 or all of them 18.14 to show that $B = [\bar{1}2\bar{3}]$.

Finally, use the [001] stereographic projection. Draw a great circle that passes through the (111), $(2\bar{1}0)$ and $(\bar{3}31)$ points using your Wulff net: they all lie on one great circle because they are in the same zone. Now identify the zone axis directly by measuring 90° from all the poles. The result is, of course, the same in each case.

- Notice that if you used the stereographic technique with a non-cubic material, you would locate a direction, not a plane normal.
- You can make the determination of **B** more accurate by making $\mathbf{s} = 0$ for each reflection you use and then estimating your deviation from this idealized orientation. If the specimen is thicker, use Kikuchi lines (Chapter 19).

18.11 ORIENTATION RELATIONSHIPS

Once you've learned how to index a DP and determine **B**, you can determine *orientation relationships (ORs)*, which are one of the most useful aspects of diffraction in the TEM for the materials scientist and nanotechnologist because the orientation between different grains, phases or crystals controls many properties of engineering materials. For example, the OR will determine how well the atomic planes in two different phases or grains fit together and this controls the nature of the interphase interface (e.g., coherent or incoherent) or grain boundary (special or random) which, in turn, governs the ways dislocations interact with the planar defect, thus controlling the mechanical behavior of the material. There are many other such effects of ORs; for example, we often want to know how a fiber is oriented to the surrounding matrix, a nanoparticle or a thin film to its supporting substrate. So the OR between two different crystals is important in many materials and can be described in one of two ways

- Two directions or plane normals (or two sets of parallel planes) can be parallel in the two crystals (the parallel-plane/direction relationship). We use this description for precipitate-matrix ($\beta - \alpha$) orientation relationships where the crystal systems may be different.
- The two crystals have a common direction (axis) so that one crystal can be rotated through some angle

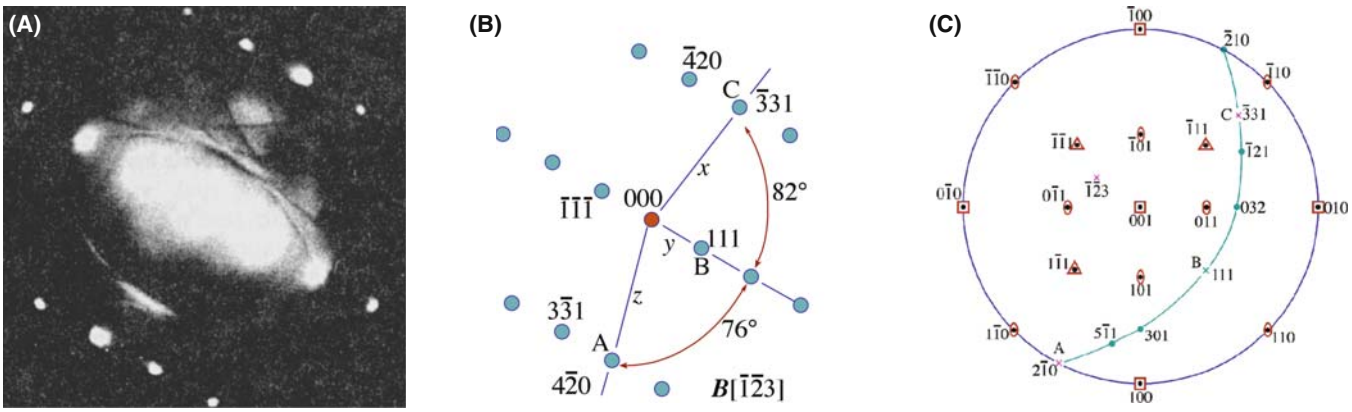

FIGURE 18.22. (A) An fcc pattern, indexed in (B) with the major indexed poles plotted on a stereographic projection in (C), identifying the pole of the great circle as $\bar{1}23$ which is therefore the beam direction for the pattern in (A).

into exact alignment with the other (an axis-angle pair). We use this for GBs where the same material is present, either side of the boundary.

Record a set of three DPs, one from each crystal and one including the interface. If you're lucky you'll be able to index both single-crystal patterns directly. If one of them shows too few spots, you should try to record a complementary Kikuchi pattern (next chapter) or CBED pattern (subsequent two chapters) to provide more information. With CBED patterns from very small regions, you'll have to take a pattern in one crystal, translate the specimen or traverse the beam and take another pattern from the other grain.

We'll go through the experimental steps for analyzing the parallel-plane/direction relationship for two phases α and β

- Tilt to the zone-axis pattern (ZAP) 1 in phase α, the matrix phase. Record and index it to determine $\mathbf{B}_1(\alpha)$.
- Translate the precipitate, β, onto the axis without touching the beam-tilt controls and record another DP. This pattern may not be exactly on a zone axis, so it may be more difficult to index; then Kikuchi lines may help considerably. Nevertheless, you need to determine a parallel-beam direction, $\mathbf{B}_1(\beta)$, for the precipitate.
- Translate back to the matrix. Tilt the specimen in a known direction until you find a different ZAP (again, Kikuchi maps will help you do this). Record and index ZAP 2 to give $\mathbf{B}_2(\alpha)$.
- Translate back to the precipitate, record the DP and index it, giving you $\mathbf{B}_2(\beta)$.
- Plot the position of $\mathbf{B}_1$ and $\mathbf{B}_2$ for both α and β on a stereogram and construct the poles of the important planes that are normal to each **B**. These will be the low-index planes that you indexed in each pattern.

So now you know that $\mathbf{B}_1(\alpha)$ is parallel to $\mathbf{B}_1(\beta)$ and $\mathbf{B}_2(\alpha)$ is parallel to $\mathbf{B}_2(\beta)$. You can also see which plane normals are parallel (if any) from the stereogram. So you can quote the OR in terms of these two pairs of parallel directions, or a pair of directions and a pair of plane normals in the zone of each **B**. It may well be the case that you can't find two low-index planes or directions that are parallel, in which case the orientation relationship is not a strong one. However, there are some well-known ORs between phases that you should know

- Best known is the *cube*/*cube* OR. If an fcc precipitate forms inside an fcc matrix (e.g., Al_3Li (δ') in an Al-Li (α) solid solution), then we find:

  $[100]_{\delta'}$ is parallel to $[100]_{\alpha}$,
  $(010)_{\delta'}$ is parallel to $(010)_{\alpha}$.

  Obviously, in these circumstances, any two $<UVW>$ directions or $\{hkl\}$ planes in the cubic system would be parallel. It's just convention to choose the lowest-index planes or directions to define the OR. When the lowest-index planes and directions align, the surface energy between the phases tends to be lowest, so this configuration is thermodynamically favored.
- The Kurdjumov-Sachs OR is often found relating fcc and bcc crystalline grains. The close-packed planes (or closest packed in bcc) and close-packed directions are parallel, but these are not now identical

  $(111)_{fcc}$ is parallel to $(011)_{bcc}$ (the closest-packed planes),
  $[10\bar{1}]_{fcc}$ is parallel to $[11\bar{1}]_{bcc}$ (the close-packed directions),
  $(\bar{1}2\bar{1})_{fcc}$ is parallel to $(\bar{2}1\bar{1})_{bcc}$.
- The Nishiyama–Wassermann OR is related to the Kurdjumov–Sachs OR

  $[0\bar{1}1]_{fcc}$ is parallel to $[001]_{bcc}$,
  $(\bar{1}11)_{fcc}$ is parallel to $(\bar{1}10)_{bcc}$ (the closest-packed planes),
  $(211)_{fcc}$ is parallel to $(110)_{bcc}$.

If you plot this out on a stereogram, you'll see it's only a few degrees away from the Kurdjumov–Sachs relationship.

- The fcc and hcp systems also share an OR in which the close-packed planes and directions are parallel:

  $(111)_{fcc}$ is parallel to $(0001)_{hcp}$ (the close-packed planes),
  $[1\bar{1}0]_{fcc}$ is parallel to $[1\bar{2}10]_{hcp}$ (the close-packed directions).

If you want to determine an axis-angle pair you proceed in a similar way. Obtain two indexed beam directions, $\mathbf{B}_1$ and $\mathbf{B}_2$, in each crystal, and plot them on a stereogram. Then you need to determine from the stereogram which angle brings the directions and planes from one crystal into coincidence with the other crystal.

There's a full discussion of these methods in Edington's text; Randle and Ralph summarize the various methods available to determine boundary crystallography and many more examples of ORs are described in the companion text.

18.12 COMPUTER ANALYSIS

Although you must be able to analyze and index DPs 'by hand,' it's likely that you'll use one of the many available software packages, especially if your specimen is not cubic (see, e.g., Section 1.6 and URLs #1, 4–7). The main challenge comes when you have to index the

DP of a new material. Your laboratory should have the standard reference sources listed at the end of the chapter. The approach simply requires that you collect all the data you can and then search through the ICDD powder diffraction files, or better still the NIST/Sandia/ICPD electron-diffraction database (see URL #5), until you find a match. Yes, it is a lot of work and you have to remember some rules

- Measurements made on calibrated SADPs will be accurate to 1–2%. If you think you're more accurate, you may eliminate the material you're seeking from your database search!
- Check for multiple domains and double diffraction first. A schematic of such a DP is shown in Figure 18.23. As you can appreciate from the schematic, you must be careful not to confuse such patterns with those showing systematic absences.

A strategy for search-and-match procedures has been given by Lyman and Carr. The goal of the exercise is to identify all the possible compounds that could produce your DP. Then you can use other data (e.g., the chemistry deduced by XEDS or EELS) to make the final identification. Computers not only give us the speed to make such

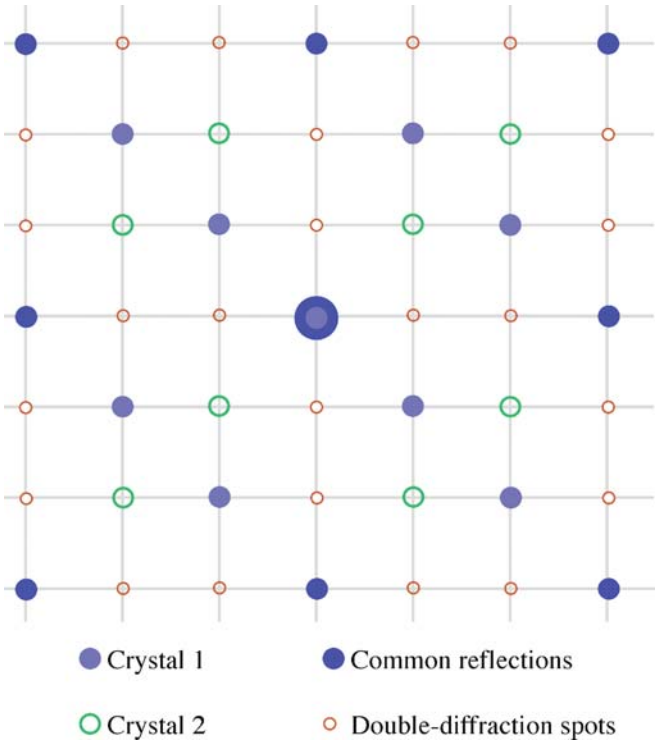

FIGURE 18.23. Care is needed to recognize diffraction from two similar domains which appears identical to diffraction from a real structure with a different symmetry. All the spots lie on a square array which may lead to erroneous indexing as a 100 pattern. The DP actually consists of separate patterns from two overlapping crystals plus double-diffraction spots as indicated.

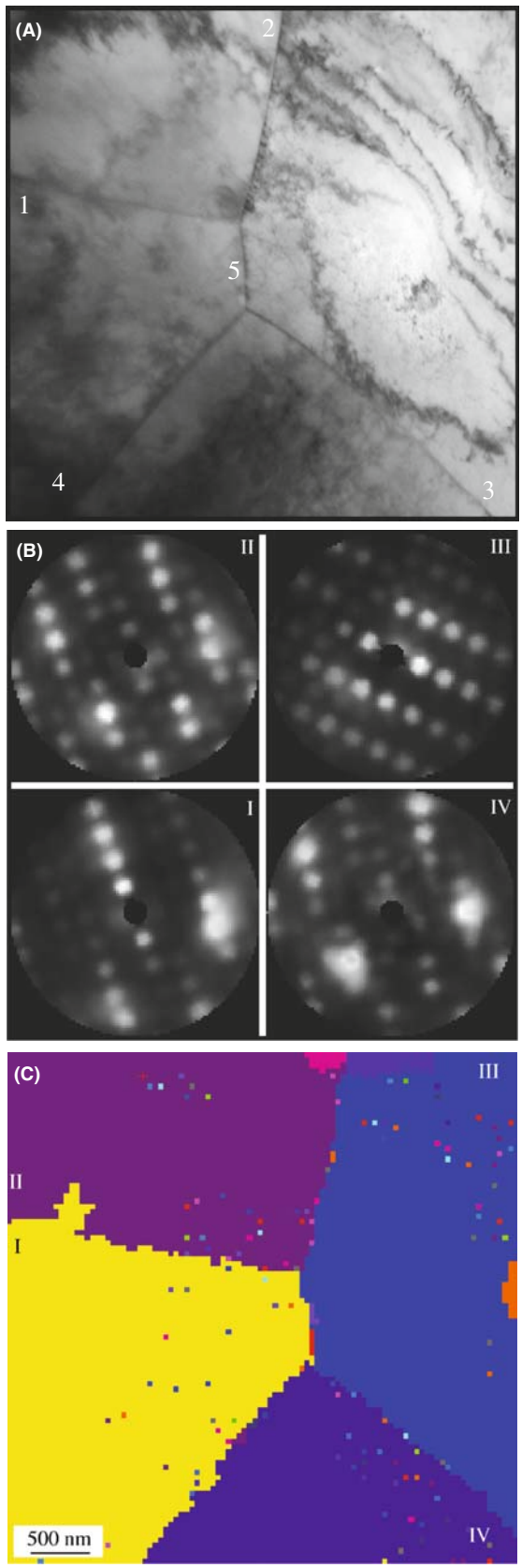

FIGURE 18.24. (A) STEM BF image of four grains in Cu. (B) A set of DPs produced from the grains as the beam scans across them. (C) A grain-orientation map in which different colors relate to different crystal orientations with respect to beam direction.

searches possible, but are also more objective. The procedure has four simple steps

- Obtain reliable data (and do not be too optimistic or overconfident in your accuracy).
- Search the database for possible matches. With the right database, chemical information will help.
- Test the matches you find. Are any of them possible given what you know about your specimen?
- Confirm the identification. Now you can go back to the microscope and use CBED to explore symmetry elements, improve your lattice-parameter measurements, etc. (Chapters 20 and 21).
- You should also simulate the DPs to confirm that the popular software packages do reproduce what you see. It's not a bad idea to carry out this exercise up front using known areas of your specimen or standard specimens before you attack the identification of unknowns.

18.13 AUTOMATED ORIENTATION DETERMINATION AND ORIENTATION MAPPING

In a parallel way to EBSD patterns in the SEM, a sequence of computer-indexed DPs can be transformed into an orientation map, which is an image in which the contrast or color links areas of similar orientation. One way to do this is via Automated Crystallography for TEM (ACT) developed by Dingley and available commercially via EDAX. ACT gives you on-line orientation determination using hollow-cone DF imaging. As shown back in Figure 9.15A, the beam is tilted and rotated by the scan coils and strong diffracted beams travel sequentially down the optic axis as individual Bragg reflections occur. Digital DF images are collected at each beam position by an on-axis CCD camera as each grain diffracts at different orientations and a parallel-beam SADP is built up.

When the incident beam satisfies the Bragg condition for a given grain, the corresponding area in the DF image appears bright. After scanning, the recorded DF images are examined. In the DF images, recorded at different incident-beam positions, a specific pixel always corresponds to the same area in the specimen. The intensity of each pixel can be drawn as a function of beam tilt and rotation angle (i.e., a DP). Adjacent pixels having the same DP are from the same grain, and thus a grain map can be built. Figure 18.24A shows four grains with five grain boundaries in a specimen of Cu. Figure 18.24B shows a set of reconstructed DPs from four grains (I–IV). Once the DPs for all the grains are reconstructed, the orientation relationships across the boundaries (1–5) between the neighboring grains can be extracted and Figure 18.24C shows the orientation map for the four grains. As in the SEM it is easy to contemplate combining the diffraction data with elemental data gathered by XEDS and/or EELS and carrying out on-line phase identification.

CHAPTER SUMMARY

This chapter has been concerned almost entirely with experimental technique.

- The stereographic projection is a very helpful aid. It's similar to projections we use to map the earth. Diffraction space (like global space) is three-dimensional. The stereographic projection gives us a two-dimensional map to guide us from pole to pole!
- How do you obtain the best DP from your specimen? Use the right exposure, always focus the DP and use the best technique (CBED or SAD ± Kikuchis) for the size of the area of interest.
- Take the trouble and time always to get good DPs. You never know when you'll really need that information and an extra 9 or 29 seconds exposure time is not long, considering how long you'll spend analyzing the results!
- Which type of DP should you use? This depends on the characteristics of your specimen and what you want to know.
- Remember that reflections with moderately large values of $\mathbf{g}$ should give you the best value for both d and ϕ, but *be absolutely sure* that $\mathbf{s} = 0$ for your chosen $\mathbf{g}$.
- DPs from polycrystalline, nanocrystalline and amorphous materials contain a wealth of information. The added value that the various TEM techniques bring over X-ray diffraction is the spatial resolution and the accompanying images. TEM may not give the best statistics; XRD only gives statistics.

- Computer indexing of DPs should be the norm and should be automatic *if you know your material*. If you understand the principles discussed here, you will avoid a few pitfalls.
- Computer control of the beam and computer indexing can also be combined to form orientation maps of the distribution of different grain orientations or textures.

Finally, we'll repeat our word of caution: there is a very famous paper on interstitial defects in a ceramic and a follow-up paper on vacancy defects. The first paper missed the 180° ambiguity in the DP! Don't fall into such good company.

REFERENCES

We list more references than usual in this chapter. You'll want to see many different examples so go to the originals where possible.

CRYSTALLOGRAPHY AND DIFFRACTION

Andrews, KW, Dyson, DJ and Keown, SR 1971 *Interpretation of Electron Diffraction Patterns* 2nd Ed. Plenum Press New York. An essential resource for anyone using electron diffraction.

Burger, MJ 1978 *Elementary Crystallography* MIT Press Cambridge Massachusetts. One of the classics. Find it in the library.

Champness, PE 2001 *Electron Diffraction in the TEM* Bios (RMS) Oxford UK. Superb, concise introductory text; full of great examples.

Cullity, BD and Stock, SR 2001 *Elements of X-ray Diffraction* 3rd Ed. Prentice-Hall New York. The standard text on XRD.

Edington, JW 1976 *Practical Electron Microscopy in Materials Science* Van Nostrand-Reinhold New York. Part 2 of the book is full of useful hints and examples on analyzing DPs.

Giacovazzo, C, Monaco, HL, Artioli, G, Viterbo, D, Ferraris, G, Gilli, G, Zanotti, G and Catti, M 2002 *Fundamentals of Crystallography* 2nd Ed. Oxford University Press and IUCr Oxford. A comprehensive reference book.

Glazer, AM 1987 *The Structure of Crystals* Adam Hilger Bristol United Kingdom. The essentials condensed into a 50-page monograph. Find it in the library

Hammond, C 1992 *Introduction to Crystallography* 2nd Ed. Royal Microscopical Society Oxford United Kingdom. An excellent compact introduction to the subject with a nice section on the biographies of crystallographers.

Johari, O and Thomas, G 1969 *The Stereographic Projection and Its Applications in Techniques of Metals Research* Ed. RF Bunshah Interscience New York. A very helpful book if you can find a copy in your library (it's out of print).

Kelly, A, Groves, GW and Kidd, P 2000 *Crystallography and Crystal Defects* Wiley New York. Update of the classic 1970 edition. All materials scientists should already have one on their shelves. Not only the standard introductory text on this subject but also gives a good review of the stereographic projection.

Klein, C and Hurlbut, CS 1985 *Manual of Mineralogy* Wiley New York. This is the modern version of the original classic by James D Dana. It gives an excellent readable review of the stereographic projection and its relation to the globe, plus basic crystallography.

Lisle, RJ and Leyshon, PR 2004 *Stereographic Projection Techniques for Geologists and Civil Engineers* 2nd Ed. Cambridge University Press New York.

Smaill, JS 1972 *Metallurgical Stereographic Projections* Adam Hilger Ltd London. Chapter 20 is another source for stereographic projections and the Wulff net if you can find a copy.

Vainshtein, BK 1981 *Modern Crystallography* **1**–**IV** Springer-Verlag New York. No longer modern but more of a classic.

Villars, P and Calvert, LD 1991 *Pearson's Handbook of Crystallographic Data for Intermetallic Phases* 2nd Ed. ASM Metals Park Ohio. This text is now in many volumes covering an ever-growing number of materials.

Wells, AF 1984 *Structural Inorganic Chemistry* 6th Ed. Oxford University Press New York. The source for crystal-structure data in inorganic materials.

AMORPHOUS MATERIALS

Graczyk, JF and Chaudhari, P 1973 *A Scanning Electron Diffraction Study of Vapor-Deposited and Ion Implanted Thin Films of Ge. I* Phys. Stat. Sol. **B58** 163–179. Early modeling; you should check other papers by these authors if you're working in this area.

Howie, A 1988 in *High-Resolution Transmission Microscopy and Associated Techniques* p 607 Eds. P Buseck, J Cowley and L Eyring Oxford University Press New York. On amorphous materials.

McCulloch, DG, McKenzie, DR, Goringe, CM, Cockayne, DJH, McBride, W, Green, DC 1999 *Experimental and Theoretical Characterization of Structure in Thin Disordered Films* Acta Cryst. **A55**(2) 178–187.

Rudee, ML and Howie, A 1972 *The Structure of Amorphous Si and Ge* Phil. Mag. **25** 1001–1007.

Treacy, MMJ, Gibson, JM, Fan, L, Paterson, DJ and McNulty, I 2005 *Fluctuation Microscopy: a Probe of Medium Range Order* Rep. Prog. Phys. **68** 2899–2944.

DIFFRACTION TECHNIQUES

Dingley, DJ 2000 in *Electron Backscatter Diffraction in Materials Science* p1 Eds. AJ Schwartz, M Kumar and BL Adams Kluwer New York.

Lyman, CE and Carr, MJ 1992 in *Electron Diffraction Techniques* **2** p 373 Ed. JM Cowley Oxford University Press New York.

Morniroli, JP, Redjaimia, A and Nicolopoulos, S 2007 *Contribution of Electron Precession to the Identification of the Space Group from Microdiffraction Patterns* Ultramicroscopy **107** 514–522.

Own, CS, Marks, LD and Sinkler, W *Electron Precession: a Guide for Implementation* Rev. Sci. Instrum. 2005 **76** 33703-1-13.

Randle, V and Ralph, B 1986 *A Practical Approach to the Determination of the Crystallography of Grain Boundaries* J. Mater. Sci. **21** 3823–3828.

Schwartz, AJ, Kumar, M and Adams, BL (Eds.) 2000 *Electron Backscatter Diffraction in Materials Science* Kluwer New York.

Tietz, LA, Carter, CB and McKernan, S 1995 *Top-Bottom Effects in Double Diffraction* Ultramicroscopy **60** 241–246. A challenge on 'double diffraction.'

Vainshtein, BK, Zuyagin, BB and Avilov, AV 1992 in *Electron Diffraction Techniques* **1** p 216 Ed. JM Cowley Oxford University Press New York.

Vincent, R and Midgley, PA 1994 *Double Conical Beam-Rocking System for Measurement of Integrated Electron Diffraction Intensities* Ultramicroscopy **53** 271–282. Precession diffraction.

URLs

1) Diffraction-Pattern Indexing – Start with the EM Yellow Pages and the EMS software http://cimewww.epfl.ch/EMYP/emyp.html and also the Web site for the International Union of Crystallography http://journals.iucr.org/iucr-top/comm/ced/index.html. Also try SingleCrystal™; part of the extensive CrystalMaker® suite of DP and crystal structure software. For a free demo download go to www.crystalmaker.co.uk/singlecrystal/index.html.
2) www.jcrystal.com/products/winwulff/index.htm – WinWulff: a program for plotting stereographic projections onto a Wulff net.
3) www.nanomegas.com – Commercial retrofit for precession diffraction.
4) www.icdd.com – ICDD Powder Diffraction File is produced by the International Center for Diffraction Data (12 Campus Boulevard, Newtown Square, PA 19073). The latest installment of the historic Powder Diffraction File, Release 2006 contains data from the ICDD experimental powder data collection and data collected, edited and standardized from NIST and ICSD database in CD/DVD formats. Expensive, but your university or research lab should buy access.
5) http://icsd.ill.fr/icsd/index.html – Inorganic Crystal-Structure Database (ICSD): the world's most extensive database on inorganic crystal structures and contains information on all inorganic crystal structures (pure elements, minerals, metals and intermetallic compounds, including their atomic coordinates) that have been published since 1913. It is updated twice a year, each time adding approximately 3000 new records. Unlicensed users only have access to a demonstration version, with a 3592 structure subset of the 93,720 inorganic structures in release 2006-2. Access also comes with the ICDD CD.
6) http://icsd.ill.fr/icsd/index.html – NIST Crystal Data comprise standard cell parameters, cell volume, space-group number and symbol, calculated density, chemical formula, chemical name and classification by chemical type. The file includes reliable data from solid-state materials including inorganics, organics, minerals, intermetallics, metals and alloys. Comprehensive chemical, crystallographic and identification search software comes with the database. Access is also available via the ICDD CD.
7) http://www.nist.gov/srd/nist15.htm – NIST/Sandia/ICDD Electron Diffraction Database is thanks to the tireless efforts of M Carr. Designed for phase characterization by electron diffraction, this database and software permit highly selective identification of microscopic and macroscopic crystalline materials.

The database contains chemical, physical and crystallographic information on over 81,534 minerals, metals, intermetallics and general inorganic compounds. Available in CD-ROM format.

THE COMPANION TEXT

Your skill in indexing diffraction patterns always benefits from practice. Energy filtering can improve the clarity of your DP but the geometry will be the same.

SELF-ASSESSMENT QUESTIONS

Q18.1 At what grain size does SAD begin to become useful?
Q18.2 How would you excite a higher-order reflection?
Q18.3 Why is it useful to use stereographic projections when analyzing DPs?
Q18.4 In a stereographic projection, are the small or great circles similar to (a) latitude, (b) longitude?
Q18.5 On the stereographic projection, if the zone axis is at the center of the circle, where are the poles of the planes in the zone?
Q18.6 What kind of ring is seen in the DP from a large-grained polycrystal?
Q18.7 How can we distinguish polycrystalline rings in the DP from those that would be caused by amorphous materials?
Q18.8 Why does double diffraction complicate understanding a DP?
Q18.9 When would you prefer SAD over CBED and vice versa?
Q18.10 Why might grains smaller than 10 nm pose a problem for diffraction analysis in the TEM?
Q18.11 How can you determine if a specimen is nanocrystalline (~1 nm grain size) or amorphous?
Q18.12 Define the radial distribution function.
Q18.13 How can you determine if a polycrystalline specimen is textured?
Q18.14 When is it a good idea to tilt the beam rather than tilt the specimen?
Q18.15 What is an orientation relationship (OR)?
Q18.16 What is the big advantages of the TEM for studying DPs?
Q18.17 How many DPs do you need to determine an OR?
Q18.18 How can you distinguish between the pattern produced by a textured specimen from one produced by a random polycrystal?
Q18.19 What is the best way to image an amorphous material?
Q18.20 Will the DP always rotate as we change the camera length?
Q18.21 Why will SAD not distinguish two patterns with 180° rotation?
Q18.22 When will double diffraction not occur?
Q18.23 What is the easiest way to examine the detail present in a DP?
Q18.24 Why do we tilt from one direction to set a selected specimen orientation?
Q18.25 Distinguish hollow cone and conical diffraction.
Q18.26 Distinguish hollow cone and precession diffraction.

TEXT-SPECIFIC QUESTIONS

T18.1 Describe how you would excite 13**g** when O is on the optic axis if you can't see 13**g** on the screen.
T18.2 Index the DPs in Figure 18.7 to be consistent with the (invisible) Kikuchi lines and with each other (after you've read Chapter 19).
T18.3 We note in Section 18.6 that, unlike those from polycrystalline materials, DPs from amorphous materials do not show speckle. However, speckle from amorphous materials is the basis for the technique of fluctuation microscopy. How can these two statements be consistent? (Use the literature and Figure 18.14 to illustrate your answer.)
T18.4 We note that indexing an OTEDP might be confusing if certain rings are missing due to the texturing. If you tilt the sample 30° these rings should reappear. Explain their absence in terms of a three-dimensional diagram like that shown in Figure 18.10D.
T18.5 Discuss which of the techniques illustrated in Figure 18.14 is better for imaging amorphous carbon. Suggest regions for the large white area in B. Why are the images in B and C different?
T18.6 Using the diagrams shown in Figure 18.17, explain the difference between Figure 18.17E and F. The argument is given in the text so try to put it into your own words or use a diagram to summarize the argument in the text.
T18.7 Is the correct B given in each of Figures 18.19A–D?
T18.8 Sketch Figures 18.21A and C on a sheet of paper so that you can describe how you would tilt from one pole to the other.
T18.9 Notice that in Figure 18.21D–F you are only told B, not the foil plane. Assuming that B is normal to the foil plane, determine the foil plane.
T18.10 Can the DP shown in Figure 18.23 actually happen? If so, give an example.

T18.11 Draw the SADP that you would obtain from a 45° [100] twist grain boundary in Cu when viewed normal to the GB plane.

T18.12 Generate the following DPs (to scale). Show all work and label reflections to a distance of 2**g** in all directions about 000. For the following, assume only 1 atom per lattice site and each lattice site contains the same atom. (A) [123] beam direction; face-centered cubic, $a = 3.68$ Å, $\lambda L = 50$ mm Å. (B) [011] beam direction; c-centered orthorhombic; $a = 4.12$ Å, $b = 3.15$ Å, $c = 5.42$ Å, $\lambda L = 50$ mm Å. (C) [113] beam direction; body-centered tetragonal; $a = 3.41$ Å, $c = 3.0$ Å, $\lambda L = 50$ mm Å. Generate the following DPs (to scale). Show all your work and label reflections to a distance of 2**g** in all directions about 000. For the following, assume only 1 atom per lattice site and each lattice site contains the same atom. (Courtesy Lucille Giannuzzi.)

T18.13 Draw the same cubic stereograms as in Figure 18.4 but rotated 90° along the horizontal axis in each case.

T18.14 Identify on Figure 18.5 the following poles: $22\bar{1}$, $01\bar{1}$, $21\bar{2}$. What is different about these three poles compared with all the others shown in Figure 18.5?

T18.15 Why are the rings of diffracted intensity in the patterns in Figure 18.9 of varying intensity? Under what conditions could you infer something about the different thicknesses of foils that gave rise to each pattern?